Controlling Electrolyte Properties and Redox Reactions Using Solvation and Implications in Battery Functions: A Mini#Review

Citation: G. Leverick, Y. Shao-Horn, Controlling Electrolyte Properties and Redox Reactions Using Solvation and Implications in Battery Functions: A Mini-Review. Adv. Energy Mater. 2023, 13, 2204094.

As Published: 10.1002/aenm.202204094

Publisher: Wiley

Persistent URL: https://hdl.handle.net/1721.1/154285

Version: Final published version: final published article, as it appeared in a journal, conference proceedings, or other formally published context

ADVANCED ENERGY MATERIALS
www.advenergymat.de

Controlling Electrolyte Properties and Redox Reactions Using Solvation and Implications in Battery Functions: A Mini-Review

Graham Leverick and Yang Shao-Horn*

Electrolytes will play a central role in the development of next-generation batteries with increased energy density and cycle life and reduced cost. While molecular designs can enable electrolytes with favorable properties like increased (electro)chemical stability, such properties can be manipulated additionally through the intermolecular interactions among species within the electrolyte. In this mini-review, a number of intermolecular interactions in the electrolyte that can give rise to significant enhancement in battery functions are highlighted. The critical role of reactant and product solubility is shown in battery reactions, where increasing solubility can enable a dissolution–precipitation reaction pathway, decrease overpotential, and increase capacity. Through the intermolecular interactions among solvent, additives, and ions, the reactivity of electrolyte species can be altered significantly by either enhancing solvent (electro)chemical stability or facilitating water deprotonation in Li–O_2 reactions. It is shown that incorporating redox active species in the electrolyte can reduce the reaction overpotential and enhance cycle life. Moreover, intermolecular interactions that can increase the ionic conductivity and transference number of electrolytes are identified. Finally, future opportunities are highlighted to exploit these intermolecular interactions to gain unprecedented molecular control over the electrolyte and enable next-generation batteries.

1. Introduction

The decarbonization of the electrical grid requires advancements in affordable, long-term energy storage to address the intermittency of energy sources like solar and wind while the continued decarbonization of the transportation sector necessitates advancements in energy dense storage devices such as batteries, with low cost and made from abundant materials.[1] Central to the function of any electrochemical device is an ionically conductive, but electronically insulating electrolyte, the ionic conductivity and transference number of which dictates the power characteristics the device.[2,3] Since the electrolyte is in contact with both electrodes, it must also exhibit a high degree of (electro) chemical stability with the electrode materials and operating voltages in order to prevent degradation reactions that limit cycle life.[4,5] The solvation properties of the electrolyte can also play a vital role in determining the reaction pathway and kinetics of conversion chemistries such as Li–S[6] and Li–O_2[6–8] batteries. Given its central role in device-level performance, electrolyte design will be critical to the development of next-generation electrochemical devices, and in fact, the next big advances in batteries will likely be driven by new electrolyte discovery. For instance, whether achieved through advances in liquid[9,10] or solid state electrolytes,[11,12] reliable Li metal batteries will likely be enabled by novel electrolytes. To facilitate these leaps forward in battery performance, deepened fundamental understanding of the molecular processes in the electrolyte is needed to enable rational design. Given that the solid electrolyte interphase (SEI) is comprised of the decomposition products of the electrolyte, what electrolyte components give rise to a stable SEI for Li metal negative electrodes? Moreover, given that Ni-rich positive electrode materials can readily decompose the electrolyte,[13,14] how do we design the electrolyte to be stable against highly reactive Ni-rich, high voltage positive electrodes? Furthermore, beyond Li-ion batteries like Li–S and Li–O_2 batteries undergo significant phase changes during charging and discharge; how do we design lean electrolyte environments and cell architectures to enable these phase transformations to occur with high active material loadings? And finally, the ionic conductivity and

G. Leverick, Y. Shao-Horn
Department of Mechanical Engineering
Massachusetts Institute of Technology
77 Massachusetts Ave, Cambridge, MA 02139, USA
E-mail: leverick@mit.edu
Y. Shao-Horn
Department of Materials Science and Engineering
Research Laboratory of Electronics
Massachusetts Institute of Technology
77 Massachusetts Ave, Cambridge, MA 02139, USA

The ORCID identification number(s) for the author(s) of this article can be found under https://doi.org/10.1002/aenm.202204094.

DOI: 10.1002/aenm.202204094

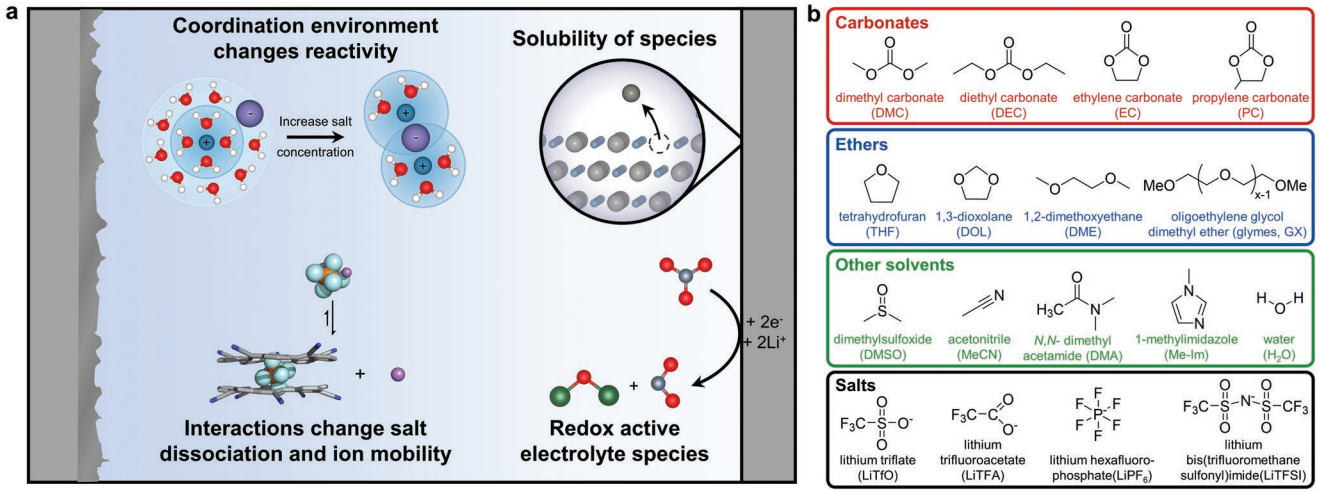

Figure 1. a) Summary of key influences that intermolecular interactions within the electrolyte can have on the performance of batteries. Images of cyanostar adapted with permission.[147] Copyright 2018, American Chemical Society. b) Summary of the chemical structures of typical solvents and salts which will be considered in this mini-review.

low transference number of conventional liquid electrolytes limits the maximum power of Li-ion batteries;[2,3] how do we enhance ionic conductivity and transference number to enable ultrafast charging and high power devices?

While the development of novel materials can enable electrolytes with enhanced properties like (electro)chemical stability and ionic conductivity, such properties can additionally be manipulated through the intermolecular interactions of species within the electrolyte. In this mini-review, we will highlight a number of critical ways that these intermolecular interactions in the electrolyte (**Figure 1**a) can give rise to significant enhancements in battery performance using known liquid electrolytes such as carbonates and ethers (Figure 1b). Such understanding, coupled with new material discovery, will be critical to enable next-generation electrolytes to enable advancements in battery performance. In Section 2, we consider how the solubility of reactants, products and reaction intermediates can influence battery reaction pathways and kinetics. In Section 3, we show the profound impact that the coordination environment of electrolyte species has on their (electro)chemical stability and reactivity. In Section 4, enhancements in performance through the use of redox active electrolyte species such as redox mediators and nitrate-based molten salts is discussed. Lastly, in Section 5, we consider how intermolecular interactions within the electrolyte can alter the ionic conductivity, as well as the ion migration mechanism.

First, we provide some theoretical background on the solvation thermodynamics of ions and experimental techniques for assessing key intermolecular interactions in the electrolyte. The solvation of Li^+ ions in aprotic electrolytes is driven largely by strong enthalpic interactions between electron donating groups on the solvent and the Li^+ ion. The solvation Gibbs free energy of Li^+ ($\Delta G^{solv}_{Li^+}$) is defined as the difference in Gibbs free energy between the solvated Li^+ and an isolated Li^+ in a vacuum[15] (**Figure 2**a). Since the energy of an isolated Li^+ in a vacuum is constant, $\Delta G^{solv}_{Li^+}$ is consequently governed by the enthalpic and entropic interactions between Li^+, the solvent, as well as other ions in the electrolyte. In aprotic electrolytes, $\Delta H^{solv}_{Li^+}$ is typically ≈−5 to −5.6 eV (Table S1, Supporting Information),[16,17] while $\Delta S^{solv}_{Li^+}$ is ≈−0.5 to −1 meV K^{-1}[16,18] ($-T\,\Delta S^{solv}_{Li^+}$ is ≈+0.15 to +0.3 eV at 25 °C, Table S2, Supporting Information), such that the solvation of Li^+ ions is driven by the strong enthalpic interactions between electron donating groups on the solvent like carbonates and ethers and Li^+. Such electron donating interactions can be well-described by solvation parameters like Gutmann donor number (DN),[19] which provide an easy-to-access value for pure solvents[20] and anions[21,22] to gauge the strength of solvent–cation and anion–cation interactions. On the other hand, the solvation of Li^+ in aprotic solvents structures the solvent molecules into a tightly bound solvation shell, which limits the entropy of Li^+ solvation to ≈−0.5 to −1 meV K^{-1}.[16,18] For instance, dimethyl sulfoxide (DMSO) forms a strong 1st solvation shell with ≈4 DMSO molecules surrounding each Li^+.[23,24] Assuming the coordination of each DMSO molecule to the Li^+ restricts its configurational entropy comparably to freezing DMSO, we can estimate the decrease of entropy caused by DMSO-coordination of Li^+ as $4 \times \Delta S_{fus} = -2.0$ meV K^{-1} (where $\Delta S_{fus} = -0.5$ meV K^{-1}[25]), which can easily account for the measured $\Delta S^{solv}_{Li^+}$ in DMSO of −0.61 meV K^{-1}.[16,18] Beyond the influence of enthalpic solvent electron donation and entropic structuring of the solvation shell, there are many other contributions to $\Delta G^{solv}_{Li^+}$ such as Coulombic and electron donor interactions between the Li^+ and anions in the electrolyte[24] and structuring of the solvent beyond the first solvation shell.[26,27] The diversity of intermolecular interactions present in the electrolyte leads to a rich design space to manipulate the solvation energy of Li^+. It is important to note that the solubility of Li salts in the electrolyte is not governed by the solvation Gibbs free energy, but rather by the dissolution Gibbs free energy (Figure 2a) which includes additional terms related to the lattice energy of the Li salt.[28] For instance, LiTFA can be dissolved to >2 M in acetonitrile (MeCN)[24] as opposed to $LiNO_3$ with solubility ≈0.3 M[29] despite the DN of TFA^- (≈34 kcal mol^{-1})[24] being higher than that of NO_3^- (DN = 21 kcal mol^{-1}),[21] which stems from the lower lattice enthalpy of LiTFA compared to $LiNO_3$ (777 kJ mol^{-1} versus 823 kJ mol^{-1} [30]).

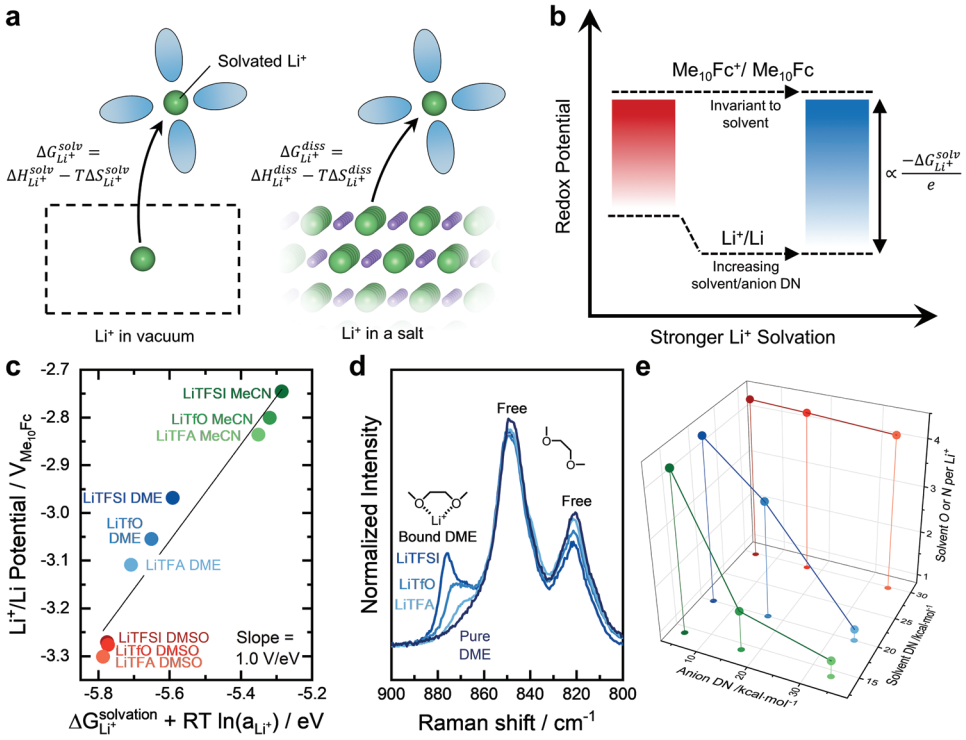

Figure 2. a) Schematic depicting the definition of the Li^+ solvation Gibbs free energy ($\Delta G^{solv}_{Li^+}$) and Li^+ dissolution Gibbs free energy ($\Delta G^{diss}_{Li^+}$). b) Depiction of how the difference between the Li^+/Li and $Me_{10}Fc^+/Me_{10}Fc$ redox potentials ($E_{Li^+/Li\ vs\ Me_{10}Fc}$) is related to the solvation Gibbs free energy ($\Delta G^{solv}_{Li^+}$), where stronger Li^+ solvation due to higher solvent or anion DN shifts the Li^+/Li potential to more negative values. c) The Li^+/Li redox potential versus $Me_{10}Fc$ plotted against reported DFT computed solvent-only Li^+ solvation strength[36] corrected by the Li^+ activity derived from ionic conductivity experiments. d) Normalized Raman spectra of 0.5 M LiTFSI, LiTfO and LiTFA mixtures in DME in the range of 800–900 cm^1. The bands at ≈876 and ≈870 cm^{-1} can be assigned to bound DME which is coordinated to Li^+, and the peaks at ≈849 and ≈821 cm^{-1} can be assigned to free (uncoordinated) DME. e) Estimated number of Li^+-coordinated solvent oxygen or nitrogen atoms in 0.5 M LiTFSI (DN = 5.4 kcal mol^{-1}[22]), LiTfO (DN = 16.9 kcal mol^{-1} [22]) and LiTFA (DN ≈ 34 kcal mol^{-1} [24]) mixtures with MeCN (DN = 14.1 kcal mol^{-1}[20]), DME (DN = 20 kcal mol^{-1} [20]) and DMSO (DN = 29.8 kcal mol^{-1} [20]). Subfigures (b), (c), and (d) reproduced with permission.[24] Copyright 2020, American Chemical Society.

The thermodynamics of Li^+ solvation can be determined experimentally through calorimetry and electrochemical measurements. The dissolution enthalpy of a Li salt (LiX) ΔH^{diss}_{LiX} is measurable using calorimetry, which can be combined with the Gibbs free energy of dissolution from the salt's solubility $\Delta G^{diss}_{LiX} = -RT\ln K$ to determine the entropy of dissolution ΔS^{diss}_{LiX}.[16] In order to isolate the single ion dissolution thermodynamics (such as $\Delta G^{diss}_{Li^+}$), an additional assumption must be made, where most commonly, tetraphenylarsonium (Ph_4As^+) and tetraphenylboride (BPh_4^-) are assumed to have identical dissolution Gibbs free energy, enthalpy and entropy.[31] Such assumption relies on the bulky phenol groups to effectively shield the influence of the charged ionic center from the surrounding solvent, and is generally considered reasonable, though differences as much as ≈8% in the solvation of Ph_4As^+ and BPh_4^- have been reported.[32] These single ion *dissolution* Gibbs free energy, enthalpy and entropy can be further related to the single ion *solvation* Gibbs free energy, enthalpy and entropy using a thermodynamic scheme based on the lattice formation energy of the dissolved salt.[33] More practically, electrolyte-dependent redox potentials such as Li^+/Li,[34] are referenced to solvent-invariant redox potentials, such as decamethylferrocene ($Me_{10}Fc$), to determine trends in the single ion Gibbs free energy of solvation. In this case, the assumption is that the solvation energy of $Me_{10}Fc$ does not change with its redox state (due to its structure shielding the redox center from the electrolyte), nor does its ionization energy change with solvation, making its redox potential constant on an absolute energy scale in all solvents.[35] With this assumption, the difference between a redox couple containing the ion of interest and that of $Me_{10}Fc$ becomes proportional to the solvation Gibbs free energy of the ion (Figure 2b). For instance, the difference between the Li^+/Li and $Me_{10}Fc^+/Me_{10}Fc$ redox potentials ($E_{Li^+/\ Li\ vs\ Me_{10}Fc}$) is related to the solvation Gibbs free energy via

$$E_{Li^+/Li\ vs\ Me_{10}Fc} = C + \frac{\Delta G^{solv}_{Li^+}}{e} \quad (1)$$

where e is the elementary charge and C is a constant given by electrolyte-independent formation energy terms where $C = -\Delta_f G^0_{Li^+} - \Delta_f G^0_{Me_{10}Fc} + \Delta_f G^0_{Me_{10}Fc^+}$ (please see the Supporting Information for full derivation). Therefore, differences in $E_{Li^+/Li\ vs\ Me_{10}Fc}$ are related linearly to changes in the Li^+ solvation energy (Equation (1)). More recently, computational techniques like density functional theory (DFT) have provided computed solvation energy of single ions, where the Li^+ solvation environment includes an explicitly defined first solvation shell (i.e., the solvent molecules are present in the calculation), which is then embedded in an implicit solvent model.[36] Remarkably,

comparing this DFT-computed Li^+ solvation energy to experimentally measured Li^+/Li redox potentials yields a strong linear correlation with a slope of 1.0 V eV^{-1} (Figure 2c), indicating quantitative agreement between these two techniques.[24,36] We further found that counter anions of increasing DN could lead to more negative $\Delta G_{Li^+}^{solv}$ in the same solvent, which can be described by the inclusion of a Li^+ activity term which was derived from ionic conductivity measurements.[24] Such findings show that the solvation energy of ions like Li^+ is governed not only by the solvent, where solvents with higher DN yield stronger solvation,[34,36] but also the counter anion where higher DN anions also strengthen Li^+ solvation.[24,37]

The solvation Gibbs free energy of Li^+ is influenced by its coordination environment, which vibrational spectroscopic techniques show consists of 4 coordinating sites coming from either just the solvent, or a combination of the counter anion and solvent. Raman spectroscopy and Fourier-transform infrared spectroscopy (FTIR) are powerful techniques for probing the ion solvation environment because solvent–ion or ion–ion interactions change shift the frequency of molecular vibrations. For instance, Raman spectroscopy taken in the 800–900 cm^{-1} range of pure 1,2-dimethoxyethane (DME) shows two broad peaks at ≈821 and ≈849 cm^{-1}, which can be assigned to mixed modes of CH_2 rocking vibrations and C–O–C stretching vibrations in oligo-ethers[24,38] (Figure 2d). Upon the addition of Li^+ salt, new bands emerge at ≈870 and ≈876 cm^{-1}, which indicate the formation of Li^+-DME complexes, where these new bands can be assigned to the vibrations of conformational combinations of the ethylene oxide chains (C–C–O) with trans (t), gauche plus (g), and gauche minus (g′) sequences.[24,39,40] Notably, the Raman scattering coefficients of these free and Li^+-coordinated solvent are nearly constant[23,24] allowing for deconvolutions of the peaks to yield quantitative information about the number of Li^+-coordinated solvent molecules. From such studies, we routinely observe ≈4 coordinating ligands per Li^+,[23,24,41] which for solvent with one coordinating ligand per solvent (like DMSO[23,24] and ethylene carbonate (EC)[41]) corresponds to 4 solvent molecules per Li^+. Through such Raman analysis, the high DN solvent DMSO retains ≈4.3 solvent oxygen atoms coordinating each Li^+ regardless of the anion DN. On the other hand, solvent coordination of the weaker DME could be increasingly displaced by anions of increasing DN from 4.3 ether O per Li^+ for $TFSI^-$ (DN = 5.4 kcal mol^{-1}[22]) to 1.1 ether O per Li^+ for TFA^- (DN ≈ 34 kcal mol^{-1}[24]) as shown in Figure 2e. Therefore, participation in the 1st solvation shell of Li^+ is a competition between the electron-donating strength of the solvent and that of the counter anion, where the higher DN species will interact with Li^+ preferentially.[24,37] Moreover, techniques such as electrospray ionization mass spectroscopy (ESI-MS)[42] and nuclear magnetic resonance (NMR)[43,44] can provide details on the solvation environment, such as the m/z of different solvated $[Li(carbonate)_n]^+$ fragments from ESI-MS studies[42] and solvent-cation interactions from ^{17}O NMR.[43,44] Unfortunately, ^7Li NMR chemical shifts (as well those of other nuclei like ^{13}C and ^1H) are not governed solely by the effective nuclear charge, where less electron density around the nucleus leads to a downfield shift. Instead, such chemical shifts can also change with the total orbital angular momenta of the valence electrons, where decreasing orbital angular momenta from reduced electron donation can induce an upfield shift.[45,46] As a result, observations from ^7Li, ^{13}C, and ^1H NMR chemical shifts should be supported using evidence from other techniques.[24]

2. Influence of Solubility on Battery Reactions

One of the simplest, yet most profound influences of electrolytes on batteries is their ability to dissolve some reactants and products, but not others. For instance, in Li-ion batteries, Li^+ ions are the only active species that is soluble in the electrolyte, while both the graphite negative electrode and lithium metal oxide positive electrode remain essentially insoluble in both their charged and discharged states. We denote such a reaction as I–I for Insoluble reactants-Insoluble products in **Figure 3**a. While this structurally simple (de)intercalation (I–I) reaction gives rise to the high rate and long cycle life of Li-ion batteries,[47] the requirement that the electrode material remain stable in both the lithiated and delithiated states imposes a limit on the electrode specific energy as heavy transition metal ions are needed to stabilize the delithiated (charged) positive electrode.[48] Conversion reactions such as Li–O_2 and Li–S, on the other hand, can offer higher specific energy, but require the electrode materials to undergo a phase transition during charge and discharge.[6–8,49] For instance, during discharge of a Li–O_2 battery, gaseous O_2 can be reduced to form insoluble solid lithium peroxide ($2Li + O_2 = Li_2O_2$, $E^0 = 2.96$ V_{Li}),[7] leading to an S–I (Soluble reactants–Insoluble products) reaction. Moreover, reaction intermediates such as lithium superoxide (LiO_2) can also be soluble in the electrolyte leading to S–(S)–I reactions (Soluble reactants–(Soluble intermediates)–Insoluble products). We next examine the manner in which the solubility of species in the electrolyte can have a profound effect on battery reactions, showing that even small solubility ≈10^{-4} M can be significant.

2.1. The Influence of Solubility on Li–O_2 Battery Reactions

The discharge of Li–O_2 batteries in aprotic electrolytes proceeds via an S–(S)–I reaction where O_2 is electrochemically reduced to a Li^+–O_2^- intermediate with limited solubility which is either further electrochemically reduced to insoluble Li_2O_2, or chemically disproportionates to form Li_2O_2 via $2\ LiO_2 \rightarrow Li_2O_2 + O_2$.[7] Solvation parameters of the electrolyte like DN[50,51] and Gutmann acceptor number (AN)[52,53] have been identified as playing a vital role in determining the discharge pathway, capacity and resulting morphology of Li–O_2 batteries. For instance, Johnson et al.[50] observed that the discharge capacity of planar electrodes showed increasing discharge capacity with increasing solvent DN, from ≈1 μAh cm^{-2} for MeCN with DN = 14.1 kcal mol^{-1}, to ≈10 μAh cm^{-2} for 1-methylimidazole (Me-Im) with DN = 47 kcal mol^{-1} (Figure 3b). Moreover, Aetukuri et al.[53] showed that adding 4000 ppm water (with high AN = 54.8 kcal mol^{-1} [19]) could increase the discharge capacity of Li–O_2 cells by ≈4 times. Work from a subset of the authors[36] consolidated these DN and AN observations to provide a universal framework for understanding the role of solvent on the discharge of Li–O_2 batteries based on the combined

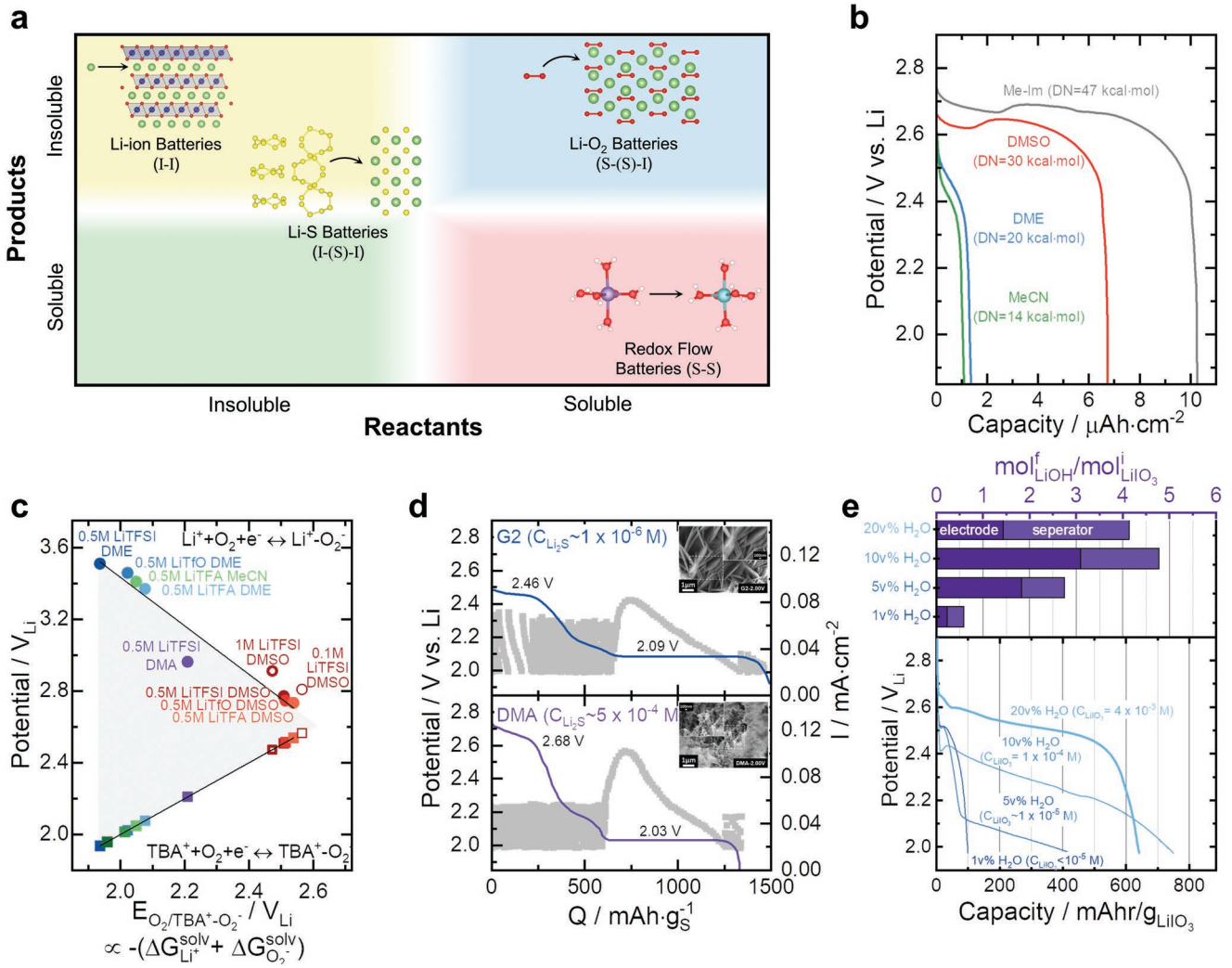

Figure 3. a) Classification of different battery chemistries based on whether the reactants, intermediates and products are soluble or insoluble. For instance, S–(S)–I refers to Soluble reactants–(Soluble intermediates)–Insoluble products. b) Discharge voltage profile of Li–O_2 planar electrodes in electrolytes of increasing DN from MeCN with DN = 14.1 kcal mol^{-1} to Me-Im with DN = 47 kcal mol^{-1}. Data from Johnson et al.[50] c) The Li^+,O_2/Li^+–O_2^- (top, circles) and TBA^+,O_2/TBA^+–O_2^- (bottom, squares) potentials on a Li^+/Li scale plotted against the TBA^+,O_2/TBA^+–O_2^- potential on the Li^+/Li scale (horizontal axis), where the horizontal axis represents the combined solvation energy of Li^+ and O_2^- ions where higher TBA^+,O_2/TBA^+–O_2^- on the Li^+/Li scale represents stronger combined solvation strength. Reproduced with permission.[24] Copyright 2020, American Chemical Society. d) GITT measurements of Li–S cells in G2 with ≈1×10^{-6} M Li_2S solubility and DMA with ≈5×10^{-2} M Li_2S solubility. Insets are SEM images of the resulting Li_2S morphology. Adapted with permission.[61] Copyright 2019, John Wiley and Sons. e) Discharge profiles of $LiIO_3$ electrodes in 0.5 M LiTFSI DME with added water from 1 to 20 vol%. Above the discharge curves are the number of moles of LiOH (mol^f_{LiOH}) from acid-base titration of the electrode (dark purple) and separator (light purple) divided by the number of moles of $LiIO_3$ in the undischarged electrode ($mol^i_{LiIO_3}$), where full conversion leads to 6 LiOH per $LiIO_3$, corresponding to 880 mAhr $g^{-1}_{LiIO_3}$. Adapted with permission.[62] Copyright 2022, American Chemical Society.

solvation energy of Li^+ (greater Li^+ solvation with higher solvent DN) and O_2^- (greater solvation with higher solvent AN). Moreover, in our follow-up work,[24] we further showed that anions of increasing DN can also strengthen the solvation of Li^+ ions, as can decreasing the salt concentration. Stronger combined solvation of Li^+ and O_2^- ions acts to weaken the interaction or coupling between Li^+ and O_2^- ions by shifting the equilibrium given by $Li^+ + O_2^- \rightleftarrows Li^+–O_2^-$ to the left. This Li^+-O_2^- coupling strength can be directly observed by comparing the difference between the Li^+,O_2/Li^+–O_2^- and TBA^+,O_2/TBA^+–O_2^- redox potentials (Figure 3c), which is related to the thermodynamic driving force of the cation exchange reaction given by $Li^+ + TBA^+O_2^- \rightarrow TBA^+ + Li^+$-$O_2^-$. With the assumption that tetrabutylammonium (TBA^+) does not interact with O_2^-, this cation exchange reaction is exactly the Li^+–O_2^- coupling strength given by $Li^+ + O_2^- \rightarrow Li^+–O_2^-$. Remarkably, from Figure 3c we see that changing the solvent from DMSO to DME increases Li^+-O_2^- coupling strength from ≈0.2 eV to almost 1.6 eV. Such changes in the combined solvation energy of Li^+ and O_2^- (which alters the Li^+–O_2^- coupling strength) can have a profound impact on the reaction pathway during discharge. Specifically, in electrolytes with very strong Li^+–O_2^- coupling, no detectable quantities of the soluble Li^+–O_2^- intermediate were observed with rotating ring disk electrode

(RRDE) measurements, consistent with a surface-mediated discharge mechanism.[50,54] On the other hand, in electrolytes with weak Li^+–O_2^- coupling, almost 80% of the discharge reaction proceeds via dissolution of a soluble Li^+–O_2^- intermediate. Unfortunately, given the transient nature of this Li^+–O_2^- intermediate, its precise solubility in the studied electrolytes is not known, though the somewhat analogous KO_2 is only soluble to ≈10^{-4} M in tetraglyme (G4).[55] We further studied the influence of Li^+–O_2^- coupling on the reaction kinetics during the discharge reaction and found that stronger Li^+–O_2^- coupling correlated with slower reaction kinetics,[24] indicating that Li^+ and O_2^- ion solvation influenced not just the reaction pathway, but also the reaction kinetics.

2.2. The Influence of Solubility on Li–S and $LiIO_3$ Batteries

Li–sulfur (Li–S) batteries discharge via a I–(S)–I reaction, during which mostly insoluble S_8 is partially reduced to soluble lithium polysulfide intermediates (such as Li_2S_8, Li_2S_6, and Li_2S_4), before being fully reduced to insoluble Li_2S.[56] Interestingly, the solubility of polysulfide intermediates has both advantages and disadvantages, where the reduction of polysulfides has been found to be more facile in instances where these polysulfides are soluble,[57] but the crossover of soluble polysulfides intermediates can impair cycle life.[58] Though widely viewed as a I–(S)–I reaction, both S_8 and Li_2S can be sparingly soluble in the electrolyte. For instance, S_8 shows a solubility ≈10^{-2} M in glymes like DME and diglyme (G2)[59,60] while Li_2S is soluble to ≈1×10^{-6} M in glymes but up to ≈5×10^{-4} M in other aprotic solvents like *N*,*N*-dimethylacetamide (DMA).[61] Even these low Li_2S solubility <1×10^{-3} M was found to significantly alter the discharge voltage and resulting product morphology of Li_2S during discharge of Li–S batteries.[61] For instance, galvanostatic intermittent titration technique (GITT) measurements of Li–S batteries showed much higher initial discharge voltage in DMA (2.68 V) with ≈5×10^{-4} M Li_2S solubility compared to G2 (2.46 V) with ≈1×10^{-6} M Li_2S solubility, as well as very different discharge morphologies (Figure 3d). Such finding highlights that solubility/insolubility is not binary, but rather exists on a spectrum (indicated by the gradients in Figure 2a), where even low species solubility (that can be challenging to detect) can potentially play a significant role in altering battery performance. We recently studied another I–(S)–I reaction based on the 6e$^-$ reduction of $LiIO_3$ to LiOH[62] which highlights the influence of reactant and product solubility on the reaction kinetics and performance of batteries with I–(S)–I discharge reactions.

Even limited reactant and product solubility <10^{-4} M can significantly enhance the discharge capacity and decrease the overpotential of $LiIO_3$ batteries. In a recent work,[62] we systematically studied the influence of solvent and the water content in the electrolyte on the 6e$^-$ reduction of $LiIO_3$ to LiOH, which proceeds via $LiIO_3 + 3H_2O + 6Li^+ + 6e^- \rightarrow LiI + 6LiOH$. The addition of water to the electrolyte had a significant effect on the solubility of both $LiIO_3$ and LiOH, such as the increasing solubility of $LiIO_3$ in DME from <1×10^{-5} M with 1 vol% H_2O to 4×10^{-3} M with 20 vol% H_2O (Figure 3e). We attributed the increasing $LiIO_3$ and LiOH solubility with increasing water content to the high solubility of $LiIO_3$ (0.8 g_{LiIO3}/g_{H2O}[63]) and LiOH (4.8 M[64]) in water due to its high AN (54.8 kcal mol^{-1}[19]) and dielectric constant (78.5[65]). Increasing the solubility of the reactant $LiIO_3$ led to a significant increase in the discharge capacity from 100 mAh g_{LiIO3}^{-1} when the $LiIO_3$ solubility was <1×10^{-5} M, to 640 mAh g_{LiIO3}^{-1} when it was ≈4×10^{-3} M (Figure 3e). Moreover, the overpotential during discharge deceased from ≈0.9 V when the $LiIO_3$ solubility was <1×10^{-5} M, to ≈0.4 V when it was 4×10^{-3} M. Remarkable is that even $LiIO_3$ solubility ≈1×10^{-5} M could enable a $LiIO_3$-dissolution discharge mechanism (Figure 3e), highlighting the profound effect that the solubility of reactants, intermediates and products can have on the discharge mechanism.

There are inherently conflicting objectives in electrolyte design for I–(S)–I battery chemistries, where increasing the solubility of species results in more facile kinetics,[57,62] but also increases the crossover of soluble species to the negative electrode.[58,66] Presently, the Li–S battery field is divided on how to resolve this conflict, with some researchers embracing the benefits of soluble polysulfides with faster kinetics while trying to suppress crossover using ceramic ion-conducting separators,[66] or by suppressing polysulfide reduction at the negative electrode.[67] Alternatively, others seek to develop electrolytes which suppress solubility as much as possible.[68,69] While determined by the intermolecular interactions within the electrolyte, the solubility of reactants, intermediates and products ultimately dictates how discharge products are deposited within the electrode, which influences the discharge capacity and resulting energy density of the cell. Regardless of the design goal, the ability to systematically design electrolytes which control the solubility of reactants, intermediates and products will play an important role in the continued development of I–(S)–I and S–I battery chemistries.

3. Altering the Reactivity of Species through Solvation Interactions

The reactivity of electrolyte species dictates critical aspects of battery performance such as cycle life. For instance, electrolyte decomposition at the positive electrode contributes significantly to poor cycle life in Li–O_2 batteries.[7,70] Work from Feng et al.[71] provided a framework for some of the key decomposition mechanisms of solvent in the Li–O_2 battery environment including hydrogen abstraction, deprotonation, nucleophilic attack and electrochemical oxidation, and identified which functional groups within the solvent structure may be vulnerable to such decomposition mechanisms. Using this framework, sulfamide- and sulfonamide-based electrolytes were developed,[72,73] which are stable against all of these decomposition pathways, as well as attack from singlet oxygen.[74] Beyond such synthetic strategies for enhancing the (electro)chemical stability of the solvent, intermolecular interaction within the electrolyte can also dramatically influence the reactivity of species, leading to enhanced solvent stability, but also enabling tuning of reactive additives like water.

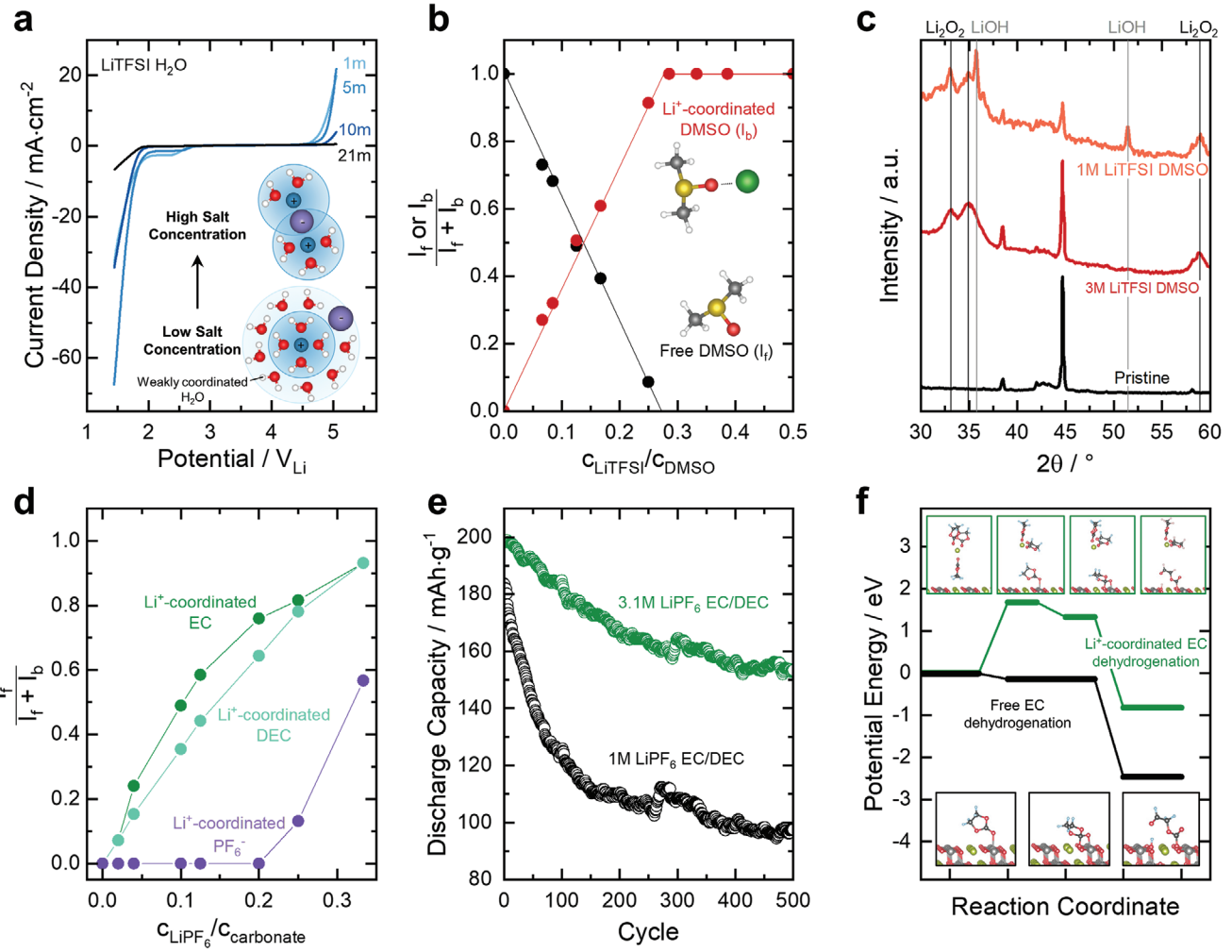

Figure 4. a) Cyclic voltammograms depicting the electrochemical stability window of LiTFSI H_2O electrolytes of different salt concentration (where m indicates mol salt per kg of solvent). Inset shows a schematic representation of the influence of increasing salt concentration on the coordination environment of water and Li^+ ions. Redrawn from Suo et al.[75] b) Proportion of free and Li^+-coordinated DMSO molecules from Raman spectroscopy as a function of the molar ratio of LiTFSI salt to DMSO. c) X-ray diffraction (XRD) of a pristine electrode, and electrodes after discharge in 1 M LiTFSI and 3 M LiTFSI. In the higher concentration 3 M LiTFSI DMSO (which has no free DMSO), there is no decomposition of DMSO to form LiOH. Subfigures (b,c) adapted with permission.[23] Copyright 2017, American Chemical Society. d) Proportion of Li^+-coordinated EC, DEC, and PF_6^- from Raman spectroscopy as a function of the molar ratio of $LiPF_6$ salt to EC/DEC solvent. e) Discharge capacity upon cycling of $LiNi_{0.8}Mn_{0.1}Co_{0.1}O_2$ cells in 1 M $LiPF_6$ EC/DEC and 3.1 M $LiPF_6$ EC/DEC show enhanced cycling stability with higher $LiPF_6$ concentration. f) Potential energy landscape from DFT calculations for the dehydrogenation of free (black) and Li^+-coordinated (green) EC. Subfigures (d–f) adapted with permission.[41] Copyright 2019, American Chemical Society.

3.1. Enhancing Solvent (Electro)Chemical Stability through Cation Coordination

Coordination between solvent molecules and cations in the electrolyte can enhance the (electro)chemical stability of the solvent. The easiest way to alter the proportion of cation-coordinated solvent molecules is by changing the stoichiometry of solvent and salt (i.e., the salt concentration). For instance, Suo et al.[75] showed a remarkable enhancement in the electrochemical stability window of aqueous electrolytes with increasing LiTFSI salt concentration (**Figure 4**a). The theoretical electrochemical stability window of H_2O is just 1.23 V, but can be extended to ≈3.0 V when the salt concentration is significantly increased to 21 m (mol salt per kg of solvent). These "highly concentrated electrolytes" (HCEs), where nearly all solvent molecules are coordinated with cations, have further shown the suppression of Al corrosion in LiTFSI-containing electrolytes,[76] graphite-compatibility with PC electrolytes[77] and even the chemical stability of MeCN against Li metal,[78] where MeCN is notorious for rapidly forming lithium cyanide in the presence of Li metal. Work from a subset of the authors[23] showed that the chemical stability of DMSO is enhanced when it is coordinated with Li^+ ions. From Raman spectroscopy, the proportion of Li^+-coordinated DMSO molecules increased ≈linearly with the molar ratio of salt to solvent until this ratio reached ≈0.25 (1 LiTFSI: 4 DMSO), after which, all DMSO molecules were found to be

coordinating Li^+ ions (Figure 4b). Critically, DMSO has been shown to be chemically unstable in Li–O_2 batteries, where DMSO can decompose via nucleophilic attack[79] or hydrogen abstraction,[80,81] consuming Li_2O_2 to form $DMSO_2$ and LiOH. However, when the salt concentration of LiTFSI in DMSO was increased such that all DMSO was coordinated with Li^+, this chemical decomposition of DMSO was suppressed, eliminating the formation of LiOH. For instance, comparing the discharge products of 1 M LiTFSI DMSO and 3 M LiTFSI DMSO from XRD, we see that the lower concentration 1 M electrolyte shows both Li_2O_2 and LiOH, whereas the highly concentrated 3 M electrolyte (which contained no free DMSO in Figure 4b), generates only Li_2O_2 (Figure 4c).

HCEs can also enhance the stability of EC in Ni-rich Li-ion batteries. Work from a subset of the authors[13,14] has identified the dehydrogenation of EC as a critical electrolyte decomposition pathway limiting the cyclability of Ni-rich Li-ion positive electrode materials such as $LiNi_{0.8}Mn_{0.1}Co_{0.1}O_2$. Critically, substituting a conventional electrolyte for a HCE where nearly all EC molecules are Li^+-coordinated can suppress this decomposition, leading to enhanced cycle life.[41] Increasing the concentration of $LiPF_6$ in EC/ethyl methyl carbonate (EMC) (3:7 w/w) led to a significant increase in the proportion of Li^+ coordinated EC and EMC, reaching >90% Li^+-solvent coordination with a molar ratio ≈0.33 $LiPF_6$:carbonate solvent (Figure 4d). Such highly concentrated $LiPF_6$ EC/EMC electrolyte showed significantly reduced solvent decomposition via diffuse reflectance infrared Fourier transform spectroscopy (DRIFTS) and X-ray photoelectron spectroscopy (XPS) measurements, as well as reduced capacity fade after 500 cycles (Figure 4e). Interestingly, this enhanced chemical stability of EC at high salt concentration did not arise due to a change in the dehydrogenation energy (which was computed to be ≈equal between free EC and Li^+-coordinated EC via DFT). Instead, Li^+ coordination with EC increased the energy barrier to chemisorption of EC onto the $LiNi_{0.8}Mn_{0.1}Co_{0.1}O_2$ surface (Figure 4f), where this chemisorption is a critical step in the dehydrogenation of EC.[82] Such finding indicates that not only can ion coordination alter (electro)chemical stability by polarizing solvent molecules and shifting their HOMO and LUMO,[83] but ion coordination can also induce kinetic limitations due to the energy barrier of desolvation.

While HCEs can increase (electro)chemical stability of the solvent, they are also hindered by their high viscosity which can decrease ionic conductivity.[84] One approach to overcome this limitation is through the dilution of the HCE with a weakly interacting solvent (sometimes called a "diluent"), giving rise to a "localized high-concentration electrolyte" or LHCE.[85,86] Notably, a well-chosen weakly interacting solvent can retain a similar coordination environment of the main solvent to that of the HCE. For instance, Chen et al.[86] found that the proportion of Li^+-coordinated dimethyl carbonate (DMC) in 5.5 M LiFSI DMC did not change upon its dilution by bis(2,2,2-trifluoroethyl) ether (BTFE), as supported by ab initio molecular dynamics (AIMD) and Raman spectroscopy. The compositional diversity offered by combining Li^+-coordinated solvent with weakly interacting diluents provides a large design space for the development of next-generation electrolytes.

3.2. Altered Electrolyte Reactivity through Solvent and Ion Interactions

The solvation environment of additives like H_2O in the electrolyte can dramatically change their reactivity. For instance, Kwabi et al.[87] compared the influence of adding 5000 ppm of H_2O to 0.1 M $LiClO_4$ DME and MeCN electrolytes during the discharge of Li–O_2 batteries. Remarkably, even though Li_2O_2 can chemically react with pure H_2O to form LiOOH and LiOH,[88] when 5000 ppm H_2O is mixed with DME, it is no longer reactive, and the discharge of a Li–O_2 battery will yield only Li_2O_2.[53,87] Such a result can be understood by considering the chemical shift of H_2O in ^1H NMR measurements, which can provide information about the acidity of the H_2O, where higher chemical shifts correspond to more acidic H_2O.[89] Significantly, the ^1H NMR chemical shift of 5000 ppm H_2O in DME is ≈2.5 ppm,[90] as compared to 4.8 ppm for bulk water,[89] suggesting that the pK_a of water in DME is higher (i.e., the water is less acidic) than bulk water. Such reduced acidity of H_2O in DME could inhibit its deprotonation by Li_2O_2, preventing the formation of LiOOH and LiOH (**Figure 5**a). On the other hand, discharge of a Li–O_2 battery with 5000 ppm H_2O in MeCN yields LiOH, not Li_2O_2,[87] indicating that the pK_a of water in solvents is solvent-dependent, where stronger solvent–water interactions (i.e., stronger dipole–dipole interactions between H_2O and neighboring solvent molecules) may facilitate the deprotonation of water.[87,91]

Ion coordination can facilitate the deprotonation of water additives in aprotic electrolytes. Previous work by the authors along with Tułodziecki et al.[90] showed that the presence of I^- ions can significantly alter the deprotonation energy of water in DME based on ^1H NMR and FTIR measurements. For instance, we showed that the chemical shift of 1000 ppm H_2O in DME could be significantly shifted from 2.44 ppm with no salt, to 4.34 with 0.3 M LiI (Figure 5b). Accompanying this change in the chemical shift of H_2O from ^1H NMR was a shift of the O–H stretching band of the H_2O in the electrolyte from 3600 cm^{-1} without salt to 3410 cm^{-1} when LiI was present, further consistent with a weakening of the OH bond of the water and more facile deprotonation (Figure 5c). Such lowered deprotonation energy of H_2O in DME with LiI altered the discharge product of Li–O_2 batteries from Li_2O_2 with no LiI, to LiOH with LiI, which was facilitated by the deprotonation of water by Li_2O_2. In follow-up work that was previously unpublished (please see the Supporting Information for experimental details), we further showed that both cations and anions could alter the deprotonation of H_2O in DME. For instance, adding $TFSI^-$ salts with alkali metal cations of increasing size, resulted in decreasing H_2O ^1H NMR chemical shift (decreasing acidity) from 3.48 ppm for Li^+, to 2.58 ppm with Rb^+ (Figure 5d), suggesting that smaller cations with higher Lewis acidity can coordinate water more strongly. Moreover, lithium halides (like LiBr and LiI) showed considerably higher H_2O ^1H NMR chemical shifts and higher H_2O acidity than other Li-salts, suggesting that Br^- and I^- ions may interact directly with H_2O in DME, whereas the other anions only serve to modulate the Li^+ activity (Figure 5e).

As with the salt concentration in HCEs above, the molar ratio of the additive to solvent and additive to ion plays a vital

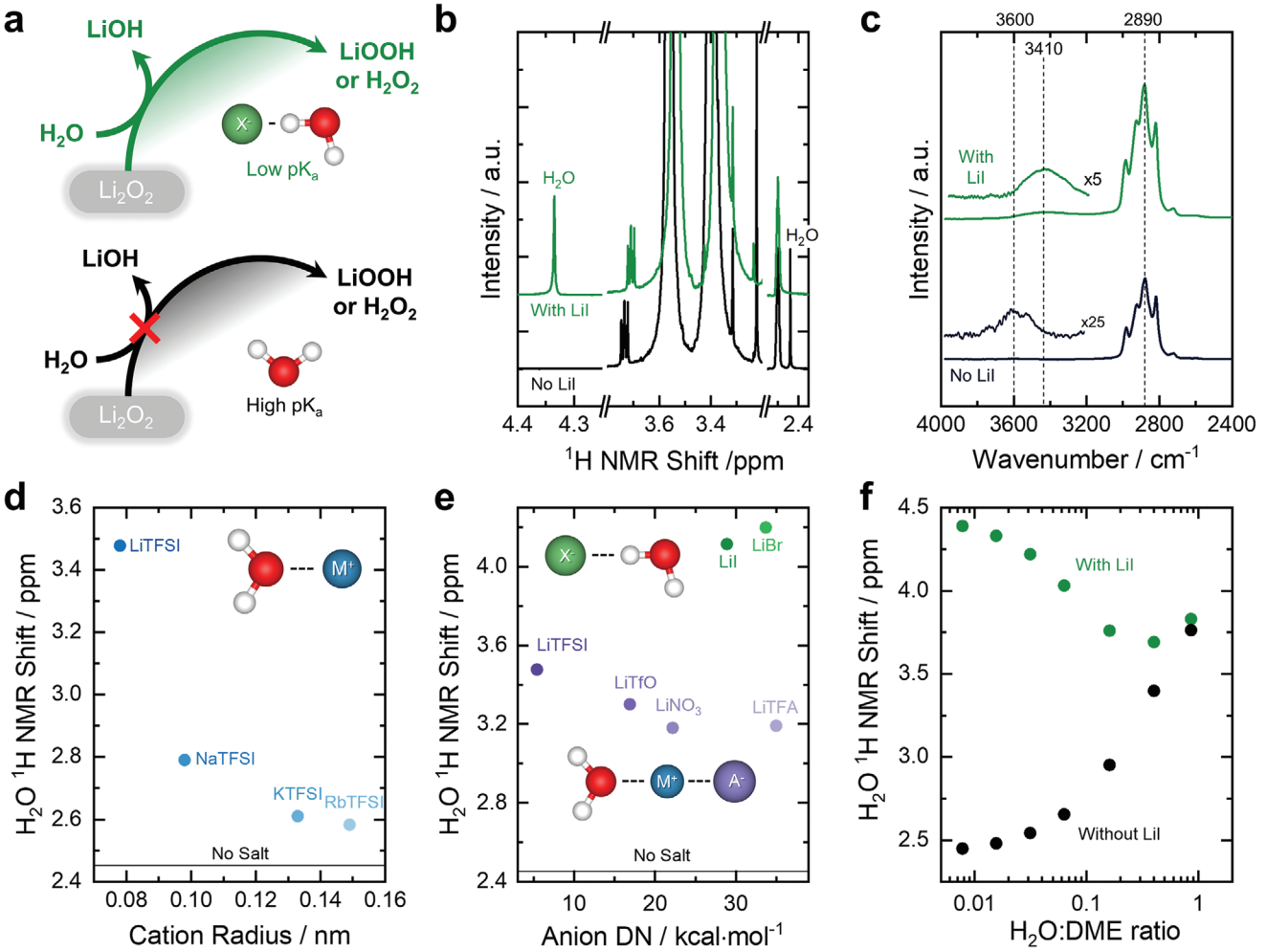

Figure 5. a) Schematic showing that when added H_2O to the electrolyte has low pK_a due to its solvation environment, it can be readily deprotonated by Li_2O_2 to form LiOH and either H_2O_2 or LiOOH, whereas when it has high pK_a, it cannot be deprotonated by Li_2O_2. b) the ^{1}HNMR spectra of DME solutions with 1000 ppm of H_2O and 0.3 M LiI and 1000 ppm of H_2O. The ^{1}H NMR signal of pure H_2O at $T = 298$ K is 4.8 ppm. c) The FT-IR spectra of pure DME with 5000 ppm H_2O and 0.3 M LiI DME 5000 ppm H_2O. d) The H_2O ^{1}H NMR chemical shift as function cation ionic radius for 0.25 M H_2O + 0.2 M MTFSI DME solutions where M = Li, Na, K, Rb. Ionic radii from Pau et al.[93] e) The H_2O ^{1}H NMR chemical shift as function anion donor number for 0.25 M H_2O + 0.2 M LiA DME solutions where A = TFSI, TfO, NO_3, TFA, I and Br. Anion DN from Linert et al.[21,22] Experimental details for subfigure d and e can be found in the Supporting Information. f) The H_2O ^{1}H NMR chemical shift as function of H_2O:DME ratios for the H_2O:DME mixture with LiI and without LiI . Subfigures (a–c,f) were adapted under the terms of the Creative Commons Attribution 3.0 International License.[90] Copyright 2017, The authors, published by RSC.

role in determining the nature of the interactions. For instance, as shown in Figure 5f, increasing the ratio of H_2O:DME from 0.008:1 to ≈1:1 increased the ^{1}H NMR chemical shift of water from 2.5 ppm to 3.8 ppm,[90] which more closely resembles the ^{1}H NMR chemical shift of bulk water (4.8 ppm[89]). Such trend can be rationalized by increasing prevalence of water-water interactions in the electrolyte with increasing water content, consistent with MD simulations by Liu et al.[89] Such dependence on the H_2O:DME ratio was also observed for LiI-containing electrolytes, where increasing the H_2O:DME ratio also increases the H_2O:LiI ratio, causing the ^{1}H NMR chemical shift of water to converge with that of the LiI-free case around ≈0.5 H_2O:DME (Figure 5f). MD simulations[89] suggest that the LiI in these LiI/H_2O/DME mixtures is concentrated in nanoscopic H_2O-rich phases, suggesting a fine balance between the ratios of these three species. Forthcoming work from the authors along with Zhang[91] et al. will further show how these H_2O:solvent ratios, as well as the nature of solvent can influence reactions such as the hydrogen evolution and reduction reaction, which is an area of significant interest.[92]

3.3. Influence of Li^+ Solvation on Graphite and Li Metal Electrodes

The solvation environment of Li^+ can enable the reversible intercalation of Li^+ into graphite, as well as influence the composition of the SEI and the resulting reversibility of Li metal negative electrodes. The graphite negative electrode in commercial Li-ion batteries is able to operate reversibly, in part, due

the presence of EC solvent in the electrolyte.[94,95] Not only does EC help to form a stable SEI,[96] but its presence in the solvation shell of Li^+ facilitates Li^+ ion desolvation, leading to reduced charge transfer resistance.[97] In fact, Ming et al.[98] have shown that even after a stable SEI has formed, facile desolvation of Li^+ ions is essential to prevent solvent co-intercalation and graphite exfoliation, where weaker solvent-Li^+ interactions help to prevent solvent co-intercalation.[99] For Li metal negative electrodes (which don't suffer from solvent co-intercalation), the composition of the SEI is determined not just by the composition of species in the electrolyte, but also whether those species are present in the solvation shell of Li^+.[100–103] This is due to the fact that the reductive decomposition of Li^+-coordinated solvent molecules is thermodynamically preferable to free solvent due to Li^+ coordination lowering the LUMO of the solvent.[104] Moreover, interactions between molecules in the solvation shell of Li^+ can further tune their reductive stability. For instance, Jiang et al.[105] have shown that additives like phloroglucinol and 1,3,5-triformylphloroglucinol can shift the LUMO of $TFSI^-$ anions in the solvation shell of Li^+ both up and down, respectively. Notably, while coordination with Li^+ ions can alter the reactivity of solvent and additives, a species being present in the solvation shell of Li^+ does not necessarily mean that it will contribute to the formation of the SEI, nor influence the resulting reversibility.[106]

Through the examples given above, it is clear that intermolecular interactions within the electrolyte can give rise to significant changes in the reactivity of electrolyte components. Given the significant demands on the electrolyte (electro)chemical stability with both the positive and negative electrodes, combining design strategies based on intermolecular interactions with synthetic strategies to select molecules that are resistant to decomposition will be critical to enable next-generation electrolytes which can delivery long cycle life. Moreover, such intermolecular interactions can enable heightened control over the reactivity of additives that participate in the reaction, such as water, enabling the development of novel beyond Li-ion chemistries with increased energy density.

4. Redox Mediators and Redox Active Molten Salt Electrolytes

The inclusion of electrolyte species that are redox active leads to even further integration of the electrolyte into the battery reactions beyond what has been discussed above. Remarkable improvements in rate and cyclability have been achieved through the incorporation of redox mediators in conversion chemistries like Li–S [107–109] and Li–O_2.[110–112] For instance, Gao et al.[110] combined 2,5-di-tert-butyl-1,4-benzoquinone (DBBQ) and 2,2,6,6-tetramethyl-1-piperidinyloxy (TEMPO) redox mediators to achieve significant rate (1 mA cm^{-2}_{geo}) and capacity (2 mAh cm^{-2}_{geo}) increases beyond electrolytes without redox mediators. Such "dual mediator"[113,114] systems showed enhanced cycle life such as a Li–O_2 batteries with stable cycling over 90 cycles reported by Liang et al.,[111] where cycling became limited by the Li metal negative electrode. Moreover, redox-active nitrate molten salts[115] have also been leveraged to enable high rate (10 mA cm^{-2}_{geo})[116] and high capacity (17 mAh cm^{-2}_{geo})[117] metal-oxygen batteries, with low overpotentials (≈0.1 V voltage difference between discharge and charge[118]) and high cycle life (>150 cycles[119]). In this section, we consider the influence of such redox active electrolyte species on the rate, reaction pathways and reversibility of Li–O_2 and Na–O_2 batteries.

4.1. Solvation Influence on Redox Mediators

Redox mediators have been widely used in Li–O_2 batteries to catalyze both the discharge[120] and charge[121] reactions. Redox mediators can be preferable to solid-state catalysts such as metal oxides[122] for promoting the charging of Li–O_2 batteries as they do not rely on good electrical contact between Li_2O_2 and the catalyst throughout the entire charging process,[123] can oxidize Li_2O_2 which forms electronically isolated from the positive electrode[124] and can suppress side reactions during charging.[123,125] Redox mediators alter the charging reaction such that the dominant pathway is no longer the electrochemical oxidation of Li_2O_2 (which is electronically insulating[126]). Instead, the redox mediator is first electrochemically oxidized at the electrode surface and then the oxidized form of the redox mediator chemically oxidizes Li_2O_2 to form Li^+ ions and molecular oxygen and regenerate the reduced form of the redox mediator. Many organic molecules like TEMPO,[127] tris[4-(diethylamino)phenyl]amine (TDPA)[128] and tetrathiofulvalene (TTF)[129] as well as inorganics like LiI[130] and LiBr[131] have been proposed as redox mediators.

The solvation strength of ions like Li^+ and I^- can dramatically alter the reactivity and reaction kinetics of redox mediators. Our recent work on redox mediators for the charging of Li–O_2 batteries has focused on LiI,[90,132] which was motivated by a number of studies suggesting high cycling stability when LiI was added to the electrolyte.[130,133] I^- ions can go through two distinct redox transitions during oxidation in aprotic electrolytes, having iodide anions (I^-) first oxidized to form triiodide (I_3^-) and I_3^- further oxidized to form iodine (I_2), where the potentials of the I^-/I_3^- and I_3^-/I_2 redox transitions can be significantly influenced by the solvent.[134] For instance, with increasing solvent AN (increasing I^- and I_3^- solvation strength), the I^-/I_3^- redox transition shifts to higher potentials versus $Me_{10}Fc$, from +20 mV in DME with AN = 10.2 kcal/mol[51] to +230 mV in DMSO with AN = 19.3 kcal mol^{-1}[51] (**Figure 6**a). We hypothesized that higher solvent AN led to a positive shift in the I^-/I_3^- redox transition (consistent with a thermodynamic preference for I^- ions over I_3^-) due to the higher charge density of I^- compared to I_3^- which could lead to stronger ion-solvent interactions. The 3:1 stoichiometry of I^-:I_3^- in the reaction ($I_3^- \leftrightarrow 3I^- + 2e^-$), could also play a role.[132] Over the same range of solvents, the I_3^-/I_2 redox transition did not shift significantly, which supports weaker interactions between I_3^- ions and the solvent, or at least similar changes in solvation energy of both I_3^- and I_2. Increasing solvation of Li^+ through increasing solvent DN can also influence the reactivity of redox mediators for charging Li–O_2 batteries.[132] For instance, increasing the solvent DN decreased the Li^+/Li potential versus $Me_{10}Fc$ from −2.96 V_{Me10Fc} for DME with DN = 20.0 kcal mol^{-1} [20] to −3.27 V_{Me10Fc} for DMSO with DN = 29.8 kcal mol^{-1} [20] (Figure 6a). Since the Gibbs free energy of gaseous O_2 (which is in equilibrium with

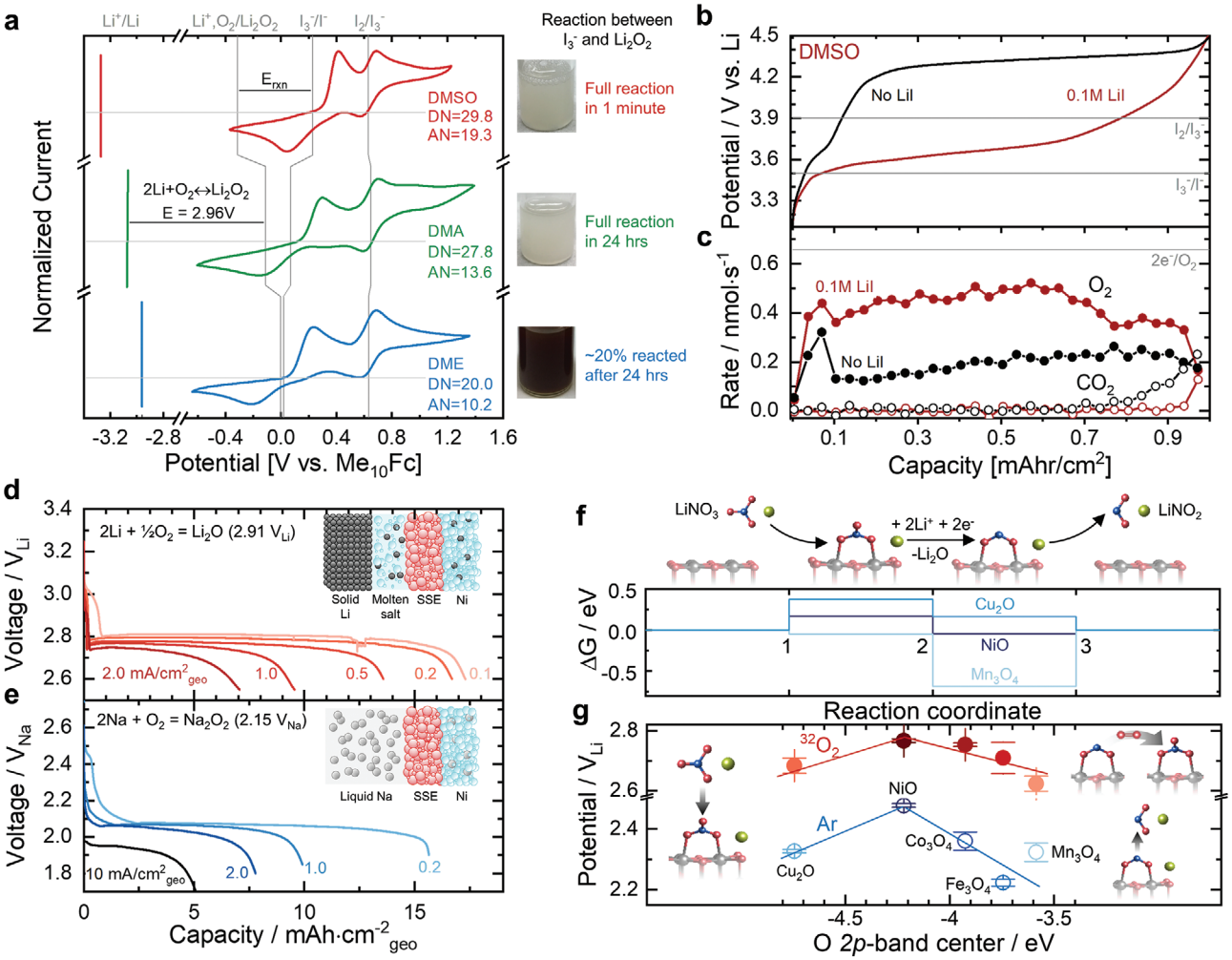

Figure 6. a) Cyclic voltammograms of solutions of 0.5 M LiTFSI + 0.1 M LiI in DME, DMA, and DMSO versus the $Me_{10}Fc$ potential. Currents were normalized based on the maximum current observed. Pictures of vial shows the electrolyte after the reaction of 0.05 M I_3^- solution (50 µmol I_3^-) to 100 µmol of Li_2O_2 where a brown color indicates the presence of unreacted I_3^-. b) Discharge profile during charging of Li–O_2 cells discharged to 1 mAh cm^{-2} in DMSO electrolytes with and without LiI added. c) Differential electrochemical mass spectroscopy (DEMS) results showing gas generation during charging of cells in subfigure b. The cell with LiI added shows increased O_2 generation and suppressed CO_2. Subfigures (a–c) reproduced with permission.[132] Copyright 2019, Elsevier. d) Discharge profile of molten-salt Li–O_2 batteries at rates of 0.1 to 2.0 mA cm^{-2}_{geo}. e) Discharge profile of molten-salt Na-O_2 batteries at rates of 0.2 to 10 mA cm^{-2}_{geo}. f) Free energy profile for the reaction $LiNO_3 + 2Li^+ + 2e^- => LiNO_2 + Li_2O$. The reduction of $LiNO_3$ to $LiNO_2$ was computed in three steps. First, NO_3^- and Li^+ adsorb onto the oxide surface to form adsorbed $–NO_3^-–Li^+$ (Step 1). Second, $–NO_2^-–Li^+$ is formed by the reaction with two Li^+ and two e^- yielding Li_2O^{NO3-} (Step 2). Third, $NO_2^-Li^+$ desorbs and dissolves into the electrolyte (Step 3). g) The volcano relation between discharge potential in O_2 (solid cycles) and Ar (open cycles) with the bulk ligand 2p-band center of formed metal oxides (Cu_2O, NiO, Co_3O_4, Fe_3O_4, Mn_3O_4) relative to the Fermi level (mid-gap for semiconducting oxides. Subfigures (d,f,g) reproduced with permission.[117] Copyright 2022, Elsevier. Subfigure (f) and insets of (e) and (f) were adapted under the terms of the Creative Commons Attribution 3.0 International License.[116] Copyright 2022, The authors, published by RSC.

dissolved O_2 in the electrolyte) and solid Li_2O_2 are solvent independent, the redox potential of $Li^+,O_2/Li_2O_2$ follows the same trend as the Li^+/Li potential,[36] decreasing from 0.00 V_{Me10Fc} in DME to –0.31 V_{Me10Fc} in DMSO. Therefore, increasing Li^+ ion solvation can be interpreted as thermodynamically destabilizing insoluble Li-compounds relative to soluble Li^+ ions on an absolute energy scale. The Gibbs free energy of the chemical oxidation of Li_2O_2 by I_3^- given by $Li_2O_2 + I_3^- \rightarrow 2Li^+ + O_2 + 3I^-$ is equal to the difference between the I_3^-/I^- and $Li^+,O_2/Li_2O_2$ redox potentials (Figure 6a). Consequently, the driving force for the reaction ΔG_{rxn} between I_3^-/I^- and Li_2O_2 became more favorable with increasing Li^+ and I^- solvation strength from –0.04 eV in DME, to –1.08 eV in DMSO. Subsequent experiments on the chemical oxidation of Li_2O_2 by I_3^- supported this trend, showing that with increasing difference between the I_3^-/I^- and $Li^+,O_2/Li_2O_2$ redox potentials, there was increasing consumption of I_3^- in the presence of Li_2O_2, as well as faster reaction kinetics (Figure 6a). Moreover, in DMSO electrolytes, where the oxidation of Li_2O_2 by I_3^- is facile, charging of Li–O_2 cells resulted in increased O_2 generation with lower voltages (Figure 6b,c), consistent with other studies.[135]

Our findings[132] highlight that the rational design of redox mediators must be done concurrently with the selection of solvent as pertinent redox couples can be shifted by up to ≈0.6 V

in different solvents (Figure 6a). Given the many other constraints on the selection of solvent, such as (electro)chemical stability[71] and ionic conductivity, not to mention the many other ways it can alter the reactions (as discussed above), it can be impractical to additionally tune the solvation of Li^+ and the redox mediator species in order to optimize its reactivity. It is, therefore, of interest to tune the oxidizing power of the redox mediators in a given solvent. It is well understood that the redox potential of organic redox mediators be shifted through systematically altering the functional groups present on the molecule.[113,136] We recently[137] introduced an approach for tuning the redox potential of halide-based inorganic redox mediators through the formation of I–Br interhalide species. We chemically formed I_3^-, I_2Br^-, IBr_2^- and Br_3^- species by mixing solutions of LiI_3 and $LiBr_3$ in DME, finding that the proportion of Br-containing interhalides increases with increasing proportions of $LiBr_3$. We showed that the interhalide IBr_2^- can form at potentials in between the I^-/I_3^- and Br^-/Br_3^- redox transitions and shows intermediate oxidizing power against Li_2O_2 compared to I_3^- and Br_3^- in chemical experiments.[137] Such interhalide species,[137] or even transition metal–halide complexes[138] can enable enhanced control over the redox potential of inorganics, to enable their reactivity as redox mediators to be tuned similarly to organic redox mediators, providing additional parameters for the design of electrolytes.

4.2. Redox Active Molten Salt Electrolytes in Metal–O_2 Batteries

Molten salts comprised of redox active nitrate anions can function as a standalone S–I battery reaction,[115] as well as a redox active electrolyte in molten-salt metal–O_2 batteries.[116,117,119,139,140] Our recent work on molten salt Li–O_2 [117] and Na-O_2[116] batteries has demonstrated that nitrate-based molten salt electrolytes can enable high performance metal–O_2 batteries. For instance, molten-salt Li–O_2 batteries with positive electrodes featuring nanoparticle Ni[117] could be discharged at rates up to 2.0 mA $cm^{-2}{}_{geo}$ with areal capacities up to 17 mAh $cm^{-2}{}_{geo}$ (Figure 6d). Moreover, by replacing the solid Li metal electrode with a liquid Na metal electrode,[116] areal rates up to 10 mA $cm^{-2}{}_{geo}$ could be achieved (Figure 6e). Such significant performance can be attributed in part to the participation of nitrate redox in the discharge reaction. For instance, using ^{18}O isotopic labelling experiments, we observed strong evidence that the formation of Li_2O in molten salt Li–O_2 batteries with transition metal oxide electrodes is formed from the reduction of NO_3^- to NO_2^- ($2LiNO_3 + 4e^- + 4Li^+ \rightarrow 2LiNO_2 + 2Li_2O$), where NO_2^- can be oxidized subsequently to NO_3^- by O_2 ($2NO_2^- + O_2 \rightarrow 2NO_3^-$), giving rise to apparent $4e^-/O_2$ reduction ($4Li^+ + 4e^- + O_2 \rightarrow 2Li_2O$). Moreover, we showed that the potential during discharge showed a volcano trend with the O 2p band center of the transition metal oxide surface. NiO catalysts showed the highest potential during discharge due to their optimal binding of both NO_3^- and NO_2^-, whereas weaker binding catalysts were limited by NO_3^- adsorption and stronger binding catalysts were limited by either NO_2^- desorption (in an O_2-free, Ar environment), or the oxidation of NO_2^- to NO_3^- by O_2 in an O_2 environment (Figure 6f,g).

As shown above, the incorporation of redox active species in the electrolyte can significantly enhance the rate capability of Li–O_2 and Na–O_2 batteries. Such strategies provide a vast design space to tune battery reactions, through the solvation strength of ions which serves to shift pertinent redox potentials, as well as tuning the redox potentials of organic and inorganic redox mediators and the inclusion of solid-state catalysts to facilitate nitrate redox. While these redox active species can greatly complicate the rational design of electrolytes, there are also significant opportunities to enable high-performance, beyond Li-ion batteries with increased energy density.

5. Enhancing Ionic Conductivity through Intermolecular Interactions

The power capability, and consequently the charging time of batteries is limited by the ionic conductivity and low transference number of conventional liquid electrolytes. During discharge (or charge), low Li^+ transference number (the contribution to overall ionic conductivity from Li^+[3]) can induce concentration gradients across the cell and within the electrodes, where active material in regions that are depleted of Li^+ ions can no longer contribute to the device capacity, imposing a limit on the power.[3,141] It is therefore of significant interest to enhance the ionic conductivity and Li^+ transference number of electrolytes to increase device power and reduce charging time. For instance, leveraging solid ceramic electrolytes with room temperature ionic conductivities of 25 mS cm^{-1} with $t_{Li+}\approx1$, Kato et al.[142] developed all solid state cells[143,144] that could be charged at 18 C, corresponding to charging ≈80% of the theoretical capacity in just 3 minutes. In this section, we examine how intermolecular interactions can give rise to the resulting ionic conductivity and transference number of electrolytes, providing pathways to enhancing device power capability.

5.1. Altering Salt Dissociation and Ion Mobility through Electrolyte Interactions

Intermolecular interactions can be used to increase the dissociation of salt ions in solvents with low dielectric constant. The influence of solvent on the ionic conductivity of electrolytes has been widely studied, where ionic conductivity can be increased by increasing the concentration of free ions (either by increasing the salt concentration or increasing the dissociation of the salt) or by decreasing the viscosity of the electrolyte which leads to faster ion mobility.[4] Unfortunately, these parameters cannot be manipulated independently as solvents with higher dielectric constant which increases salt dissociation tend to have higher viscosity[4] and increasing the salt concentration also increases the electrolyte viscosity.[84] We recently introduced a novel approach to increasing salt dissociation in low dielectric constant electrolytes where a macrocyclic anion binding receptor (Cyanostar)[145] was added to a $LiPF_6$ tetrahydrofuran (THF) ($\varepsilon_0 = 6.7$[146]) electrolyte.[147] Cyanostar (CS) exhibits size-selective anion binding and strongly binds PF_6^- anions in a 2:1 sandwich configuration (**Figure 7**). Through the addition of CS to the electrolyte, the ionic conductivity of 5×10^{-3} M $LiPF_6$ THF increased by over an order of magnitude from just 11 to 150 μS cm^{-1} (Figure 7a). Since CS is a size selective anion receptor,[145]

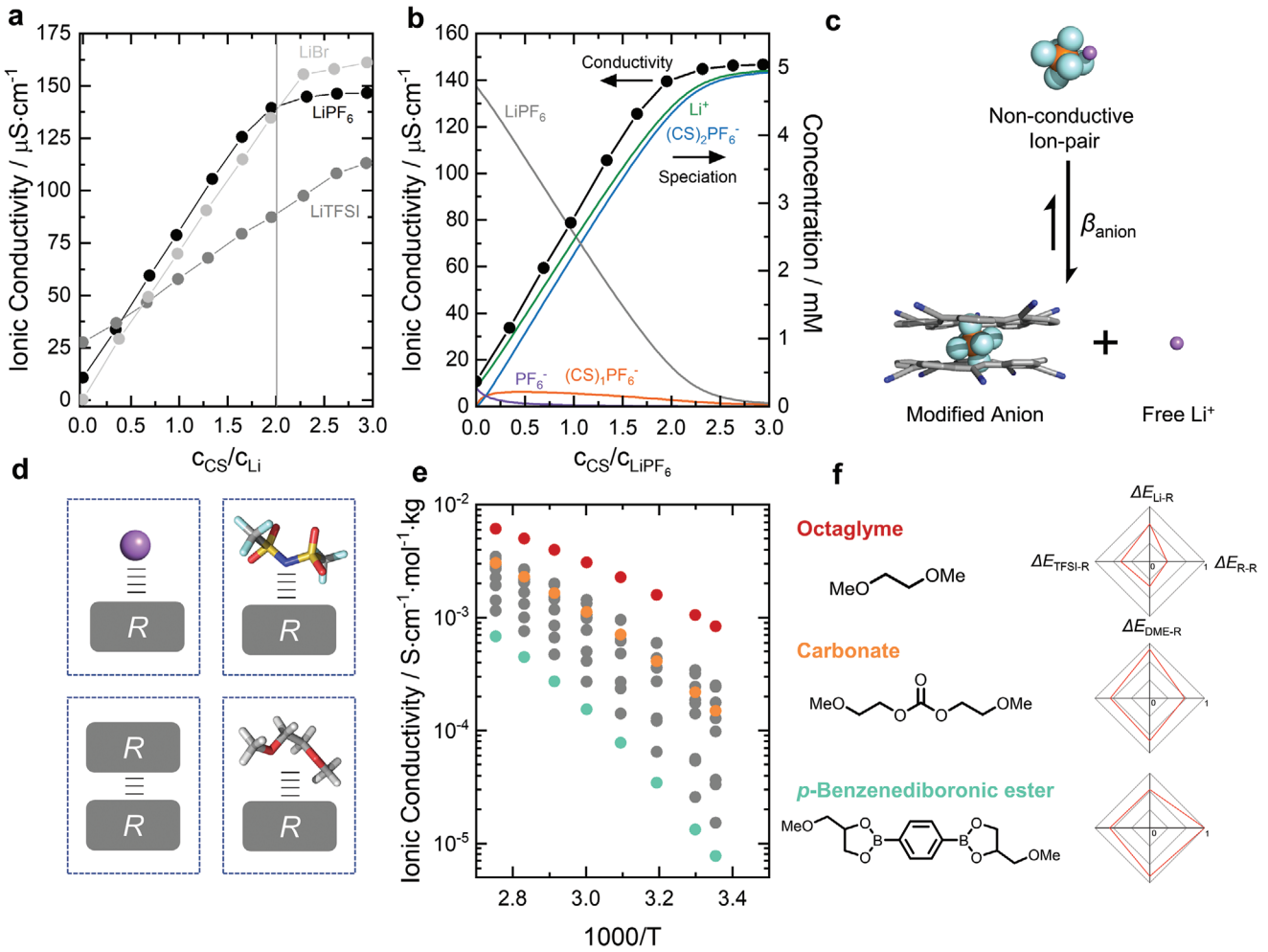

Figure 7. a) Conductivity of 5×10^{-3} M LiBr, $LiPF_6$, and LiTFSI in THF with increasing equivalents of cyanostar (CS). b) Conductivity (black dots) and the calculated concentrations (grey, green, blue, orange, and purple lines) of species formed when CS was added to $LiPF_6$. The calculation was based on a 3-equilibria model: ion paring of $LiPF_6$ (log $K_{ip} = 4.9$), CS·PF_6^- 1:1 binding (log $K_1 = 5.3$), and CS_2·PF_6^- 2:1 binding (log $\beta_{anion} = 13.5$). c) Scheme of supramolecular anion modification of ion pairs. β_{anion} is the overall association constant of the CS:anion complex. d) The pairwise interaction energies ($\Delta E_{i\text{-}R}$) of each substituent with Li^+, $TFSI^-$, DME, and itself (self-association) in the gas phase were obtained using DFT calculations and used to predict viscosity and ionic conductivity. e) Temperature-dependent molal ionic conductivities of OEG-LiTFSI electrolytes (LiTFSI, Li/O = 1/12). f) Chemical structures and normalized interaction energies of three compounds from subfigure e. The pairwise noncovalent interaction energies induced by the substituents were normalized to the maximum values within the series (e.g., $\Delta E_{Li\text{-}R}$ is normalized by dividing each energy value by the maximum $\Delta E_{Li\text{-}R}$ value within the series). Top: Li^+ interaction, $\Delta E_{Li\text{-}R}$; bottom: DME interaction, $\Delta E_{DME\text{-}R}$; left: $TFSI^-$ interaction, $\Delta E_{TFSI\text{-}R}$; right: site-site interaction, $\Delta E_{R\text{-}R}$. Subfigures (a–c) reproduced with permission.[147] Copyright 2018, American Chemical Society. Subfigures (d–f) reproduced with permission.[148] Copyright 2020, ACS.

we further probed its influence on the ionic conductivity of Li salts with different sized anions, such as LiBr and LiTFSI. 5×10^{-3} M LiBr THF (where CS shows similar binding affinity to Br^- and PF_6^-) showed a comparable trend to 5×10^{-3} M $LiPF_6$ THF, with a sharp elbow at $c_{CS}/c_{Li} = 2$ due to full coordination of all Br^- by 2 CS. On the other hand, 5×10^{-3} M LiTFSI THF showed a much more gradual increase in ionic conductivity due to weaker complexation with CS.[147] Such significant increases in ionic conductivity of $LiPF_6$ THF electrolytes could be understood by modelling the solution speciation through UV–Vis and NMR measurements of the Li^+–PF_6^- and CS–PF_6^- binding constants. This modelled speciation showed that the addition of CS increased the dissociation of $LiPF_6$ contact ion pairs resulting in high proportions of free Li^+ ions and $(CS)_2PF_6^-$ complexes (Figure 7b). The formation of these bulky $(CS)_2PF_6^-$ complexes (Figure 7c) also slowed their mobility relative to free PF_6^- leading to an increased transference number of Li^+ ions from ≈0.5 for the neat $LiPF_6$ THF electrolyte to 0.8 with two equivalents of CS.[147] Unfortunately, while this approach led to significant enhancement of salt dissociation in the low dielectric constant THF (6.7[146]), the limited solubility of CS restricted the maximum ion concentrations to $<2 \times 10^{-2}$ M.[147] Given this limitation stemming from the solubility of such macrocyclic ion binding receptors, we subsequently investigated how manipulating the solvent could change its interactions with Li^+ ions, anions as well as its self-interaction, as a means optimize electrolyte ionic conductivity and transference number.

Ionic conductivity can be relatively well-predicted based solely on the solvent-Li^+, solvent-anion and solvent-solvent interactions. We recently studied a family of selectively modified oligo-ethylene glycol (OEG) LiTFSI-based electrolytes[148] using a series of functional groups (R) with different Li–R, TFSI–R, DME–R, and R–R interactions (Figure 7d). We computed each of the pairwise interaction energies using DFT calculations for 12 different R groups. Remarkably, by fitting a nonlinear regression model that encoded an Arrhenius temperature dependence and the 4 DFT-computed pairwise interaction energies for each substituent, we could predict the temperature-dependent ionic conductivity ($R^2 = 0.98$) and viscosity ($R^2 = 0.99$) of the resulting electrolytes.[148] Such nonlinear regression model could even predict the ionic conductivity and viscosity of 3 compounds not included in the training set.[148] Such findings are significant as they illustrate that even complex macroscopic properties like ionic conductivity and viscosity are ultimately governed by simple intermolecular interactions within the electrolyte. Within our electrolyte system, R–R interaction energies (i.e., the dipole–dipole self-interactions between functional groups) were most critical in determining the resulting ionic conductivity as strong R–R interactions led to significantly increased viscosity and reduced ion mobility.[148] For instance, increasing R–R interaction energy by changing the substituent from octaglyme, to carbonate, to *p*-benzenediboronic ester resulted in decreasing room temperature molal ionic conductivity from 8×10^{-4} S cm^{-1} mol^{-1} kg^{-1}, to 1×10^{-4} S cm^{-1} mol^{-1} kg^{-1}, to 8×10^{-6} S cm^{-1} mol^{-1} kg^{-1}, respectively (Figure 7e,f).

5.2. Altering Ion Conduction Mechanisms through Electrolyte Interactions

Beyond altering the dissociation of ions and ion mobility, intermolecular interactions within the electrolyte can also alter the ionic conduction mechanism. Li^+ ion conduction in liquid electrolytes is generally thought to occur through a vehicular mechanism where the ion retains noncovalent bonds with its nearest neighbors and the first solvation shell remains fixed with respect to the solvated cation, having the cation and its solvation shell to move as a coordinated unit.[149,150] However, in some electrolytes, Li^+ ions appear to conduct through more of an ion hopping mechanism whereby the ion becomes desolvated or partially desolvated; breaking noncovalent bonds with some nearest neighbors and establishing new ones. For instance, Dokko et al.[151,152] reported a Li^+ ion hopping mechanism in highly concentrated $LiBF_4$ sulfolane (SL) electrolytes, where Li^+ had a higher diffusion coefficient than both the SL solvent and BF_4^- counter anion. Moreover, Borodin and Smith[153] leveraged MD simulations to show that solvent exchange events in the 1st solvation shell of Li^+ can occur with very different frequencies in different solvents. For example, Li^+ in LiTFSI DME electrolytes travelled almost 1.5 nm in between solvent exchange events, whereas Li^+ in LiTFSI EC exchanged a solvent molecule in its first solvation shell every 0.3 nm.[153] In work that is forthcoming,[27] we propose that the selectivity between vehicular, ion hopping and mixed ion conduction mechanisms is governed by the intermolecular interactions within the electrolyte, where a vehicular is favored when Li^+ remains tightly bound to its neighboring solvent molecules. Unleashing Li^+ ions to facilely hop through the electrolyte (analogous to the Grotthuss mechanism of proton conduction[154,155]) could enable novel liquid or polymer electrolytes which can deliver high power and fast charging.

6. Conclusions and Perspectives

In this mini-review, we have showcased the dramatic influence that the intermolecular interactions within the electrolyte can have on aspects of battery performance like discharge rate, discharge capacity and cycle life. We considered the role of reactant and product solubility on the battery reactions, showing that even low solubility $<0.1 \times 10^{-3}$ M could enable a dissolution-precipitation reaction pathway and the solubility strongly influenced the discharge overpotential and capacity. Intermolecular interactions between electrolyte components were shown to dramatically influence their reactivity, leading to significantly enhanced solvent (electro)chemical stability in highly concentrated electrolytes, and a widely tunable deprotonation energy of water. Incorporating redox active species in the electrolyte, such as with redox mediators or redox active nitrate molten salts, could significantly reduce reaction overpotentials and enhance cycle life. Finally, the ionic conductivity and transference number of electrolytes, which give rise to the power capabilities of devices, are ultimately derived from the intermolecular interactions within the electrolyte where anion-binding receptors can enhance salt dissociation, and decreasing self-interaction amongst solvent molecules can reduce viscosity and increase ion mobility.

Developing next-generation electrolytes to drive the next big leaps in battery performance necessitates unprecedented molecular control over the intermolecular interactions between electrolyte species and the solvation of ions. In Section 2, we painted an eye-opening picture whereby even small species solubility $<10^{-4}$–10^{-5} M could facilitate dissolution-based reaction mechanisms. Remarkably, such small solubility approaches the detection limits of inductively coupled plasma atomic emission spectroscopy (ICP-AES) ($\approx 1 \times 10^{-5}$ M [62]) and total dissolved solids (TDS) measurements ($\approx 1 \times 10^{-6}$ M [61]) based on ionic conductivity. Despite the importance of species with small, but nonzero solubility, relatively few works have measured the solubility of inorganic phases such as NaO_2, KO_2, Li_2S, Li_2O, and LiF. Moreover, these solubility measurements are generally performed in pure solvents, where the effect of salts and salt concentrations could have significant influence, especially in HCEs. It is therefore of significant interest to develop methodologies to probe small solubility $<10^{-5}$ M in practical electrolytes (i.e., with salt) in order to systematically study how parameters like solvent, salt concentration and counter anion influence the solubility of these phases. In addition to influencing beyond Li-ion battery chemistries like Li–O_2 and Li–S, species with nonzero solubility could influence the nucleation and growth of inorganic phases in the SEI of the negative electrode. For instance, inorganic phases such as LiF and Li_2O are widely treated as insoluble, but can be soluble up to $\approx 10^{-4}$–10^{-5} M.[29,156] Such levels of solubility, as well as the

difference in solubility between different electrolytes, could dramatically alter the nucleation and growth of these inorganic phases and the resulting properties of the SEI. For instance, smaller LiF deposits in the SEI have been correlated with higher Coulombic efficiency[157] and lower overpotentials[158] of Li metal plating and stripping. These smaller LiF deposits could, in part, stem from reduced LiF solubility in the electrolyte, promoting increased nucleation of LiF sites but reduced particle growth. Despite this, the solubility of common SEI phases such as LiF and Li_2O has only been measured in pure solvents and the solubility of other phases like lithium alkoxides and semicarbonates is unknown. By measuring the solubility of these SEI phases in practical electrolytes, the resulting influence of nonzero SEI component solubility on the nucleation and growth of the SEI can be rationally examined.

Beyond their solubility, the nucleation and growth of inorganic phases such as NaO_2, KO_2, Li_2S, Li_2O, and LiF is further altered by the kinetics of dissolution/precipitation. The kinetics of ion (de)solvation can greatly influence such dissolution/precipitation kinetics as well as electrochemical reaction kinetics during ion intercalation[91,159] and the plating/stripping of Li[160–162] and other metals. The energy barrier to Li^+ ion desolvation in carbonate electrolytes is ≈0.5–0.6 eV[163–165] based on measurements with lithium titanium oxide electrodes and DFT calculations, whereas this number can be as low as ≈0.2–0.3 eV[166] in aqueous electrolytes. Isolating the energy barrier to Li^+ ion desolvation from experimental electrochemical kinetic measurements is challenging as these reactions can be further limited by the presence of an SEI (including ion transport within the SEI and across the SEI/electrode interface), as well as the kinetics of the electrode reaction itself (such as intercalation of the desolvated ion into the electrode material).[167] Moreover, the ion and electron transfer kinetics can be coupled.[159] As a result, the molecular origin of the faster desolvation kinetics in aqueous electrolytes compared to carbonates is not understood.[167] Interestingly, these ion desolvation kinetics do not appear to correlate with the strength of ion solvation, as Li^+ is solvated more strongly in H_2O than in PC and MeCN,[168] despite Li^+ having a lower energy barrier to desolvation in H_2O than in either PC and MeCN.[169] Developing experimental methodologies that isolate the ion (de)solvation kinetics from confounding effects like the SEI and electrochemical reaction kinetics[167,169] will be critical to better elucidate the precise molecular processes occurring during ion (de)solvation, as well as to design electrolytes that enhance this process. One potential direction is through the study of salt dissolution kinetics, which can be simpler and can more directly isolate the (de) solvation of ions. Such heightened measurements and understanding of ion (de)solvation kinetics will enable the determination of key macroscopic properties such as the dissolution/precipitation rate of discharge products like Li_2S and NaO_2, as well as SEI phases like Li_2O and LiF. Precise determination of these macroscopic properties is vital to develop better models[170,171] that can inform the design of cells with high active material loading and lean electrolyte.

The next big leaps in battery performance are likely to be driven electrolyte discovery. Whether its enabling ultrafast charging through enhanced ionic conductivity and transference number, higher energy density through the stabilization of Li metal or Ni-rich electrodes, or the development of beyond Li-ion chemistries like Li–S and Li–O_2, electrolyte research is poised to play a critical role. Throughout this mini-review, we showed that not only are the molecular components of the electrolyte critical, but also the intermolecular interactions between them, giving rise to enhanced (electro)chemical stability, faster reaction kinetics and enhanced ionic conductivity. In order to rationally design next-generation electrolytes and accelerate their discovery, deeper fundamental understanding of the molecular processes involved in ion (de)solvation and the role of solubility on the SEI are required. Through developing unprecedented molecular control over the intermolecular interactions within the electrolyte, batteries with higher energy density, longer cycle life and utilizing cheaper, more earth abundant materials can be developed in order to accelerate the decarbonization of the electrical grid and the transportation sector.

Supporting Information

Supporting Information is available from the Wiley Online Library or from the author.

Acknowledgements

The work was supported in part by Shell, Toyota Motor Europe, and the Toyota Research Institute (TRI) Accelerated Materials Design and Discovery (AMDD) program. G.L. gratefully acknowledges partial support from a Natural Sciences and Engineering Research Council of Canada (NSERC) PGS-D and Siebel Scholarship (Class of 2020).

Conflict of Interest

The authors declare no conflict of interest.

Keywords

electrolytes, intermolecular interactions, lithium batteries, redox mediators, solubility, solvation

Received: November 30, 2022
Revised: January 11, 2023
Published online: February 15, 2023

[1] D. R. Rolison, L. F. Nazar, *MRS Bull.* **2011**, *36*, 486.
[2] J. Newman, K. E. Thomas, H. Hafezi, D. R. Wheeler, *J. Power Sources* **2003**, *119–121*, 838.
[3] M. Doyle, T. F. Fuller, J. Newman, *Electrochim. Acta* **1994**, *39*, 2073.
[4] K. Xu, *Chem. Rev.* **2004**, *104*, 4303.
[5] K. Xu, *Chem. Rev.* **2014**, *114*, 11503.
[6] P. G. Bruce, S. A. Freunberger, L. J. Hardwick, J.-M. Tarascon, *Nat. Mater.* **2011**, *11*, 19.
[7] D. Aurbach, B. D. McCloskey, L. F. Nazar, P. G. Bruce, *Nat. Energy* **2016**, *1*, 16128.
[8] D. G. Kwabi, N. Ortiz-Vitoriano, S. A. Freunberger, Y. Chen, N. Imanishi, P. G. Bruce, Y. Shao-Horn, *MRS Bull.* **2014**, *39*, 443.

[9] G. M. Hobold, J. Lopez, R. Guo, N. Minafra, A. Banerjee, Y. Shirley Meng, Y. Shao-Horn, B. M. Gallant, *Nat. Energy* **2021**, *6*, 951.
[10] Y. Jie, X. Ren, R. Cao, W. Cai, S. Jiao, *Adv. Funct. Mater.* **2020**, *30*, 1910777.
[11] R. Chen, Q. Li, X. Yu, L. Chen, H. Li, *Chem. Rev.* **2020**, *120*, 6820.
[12] J. C. Bachman, S. Muy, A. Grimaud, H.-H. Chang, N. Pour, S. F. Lux, O. Paschos, F. Maglia, S. Lupart, P. Lamp, L. Giordano, Y. Shao-Horn, *Chem. Rev.* **2016**, *116*, 140.
[13] Y. Yu, P. Karayaylali, Y. Katayama, L. Giordano, M. Gauthier, F. Maglia, R. Jung, I. Lund, Y. Shao-Horn, *J. Phys. Chem. C* **2018**, *122*, 27368.
[14] Y. Zhang, Y. Katayama, R. Tatara, L. Giordano, Y. Yu, D. Fraggedakis, J. G. Sun, F. Maglia, R. Jung, M. Z. Bazant, Y. Shao-Horn, *Energy Environ. Sci.* **2020**, *13*, 183.
[15] C. P. Kelly, C. J. Cramer, D. G. Truhlar, *J. Phys. Chem. B* **2007**, *111*, 408.
[16] B. Cox, G. Hedwig, A. Parker, D. Watts, *Aust. J. Chem.* **1974**, *27*, 477.
[17] Y. Marcus, *J. Chem. Soc., Faraday Trans. 1* **1987**, *83*, 339.
[18] B. G. Cox, A. J. Parker, *J. Am. Chem. Soc.* **1973**, *95*, 6879.
[19] V. Gutmann, *Electrochim. Acta* **1976**, *21*, 661.
[20] F. Cataldo, *Eur. Chem. Bull.* **2015**, *4*, 92.
[21] W. Linert, R. F. Jameson, A. Taha, *J. Chem. Soc. Dalton Trans.* **1993**, 3181.
[22] W. Linert, A. Camard, M. Armand, C. Michot, *Coord. Chem. Rev.* **2002**, *226*, 137.
[23] R. Tatara, D. G. Kwabi, T. P. Batcho, M. Tulodziecki, K. Watanabe, H.-M. Kwon, M. L. Thomas, K. Ueno, C. V. Thompson, K. Dokko, Y. Shao-Horn, M. Watanabe, *J. Phys. Chem. C* **2017**, *121*, 9162.
[24] G. Leverick, R. Tatara, S. Feng, E. Crabb, A. France-Lanord, M. Tulodziecki, J. Lopez, R. Stephens, J. C. Grossman, Y. Shao-Horn, *J. Phys. Chem. C* **2020**, *124*, 4953.
[25] H. L. Clever, E. F. Westrum, *J. Phys. Chem.* **1970**, *74*, 1309.
[26] B. Huang, S. Muy, S. Feng, Y. Katayama, Y.-C. Lu, G. Chen, Y. Shao-Horn, *Phys. Chem. Chem. Phys.* **2018**, *20*, 15680.
[27] G. Leverick, *Towards Comprehensive Design of Electrolytes for Electrochemical Energy Storage, Ph.D. Thesis*, MIT, XX **2022**.
[28] B. E. Conway, *J. Solution Chem.* **1977**, *6*, 23.
[29] N. Xin, Y. Sun, M. He, C. J. Radke, J. M. Prausnitz, *Fluid Phase Equilib.* **2018**, *461*, 1.
[30] C. K. Kim, J. Won, H. S. Kim, Y. S. Kang, H. G. Li, C. K. Kim, *J. Comput. Chem.* **2001**, *22*, 827.
[31] A. J. Parker, *Chem. Rev.* **1969**, *69*, 1.
[32] J. I. Kim, *Bull. Soc. Chim. Belges* **1986**, *95*, 435.
[33] D. R. Rosseinsky, *Chem. Rev.* **1965**, *65*, 467.
[34] G. Gritzner, *J. Phys. Chem.* **1986**, *90*, 5478.
[35] I. Noviandri, K. N. Brown, D. S. Fleming, P. T. Gulyas, P. A. Lay, A. F. Masters, L. Phillips, *J. Phys. Chem. B* **1999**, *103*, 6713.
[36] D. G. Kwabi, V. S. Bryantsev, T. P. Batcho, D. M. Itkis, C. V. Thompson, Y. Shao-Horn, *Angew. Chem., Int. Ed.* **2016**, *55*, 3129.
[37] C. M. Burke, V. Pande, A. Khetan, V. Viswanathan, B. D. McCloskey, *Proc. Natl. Acad. Sci. USA* **2015**, *112*, 9293.
[38] K. Ueno, R. Tatara, S. Tsuzuki, S. Saito, H. Doi, K. Yoshida, T. Mandai, M. Matsugami, Y. Umebayashi, K. Dokko, M. Watanabe, *Phys. Chem. Chem. Phys.* **2015**, *17*, 8248.
[39] J. Grondin, J.-C. Lassègues, M. Chami, L. Servant, D. Talaga, W. A. Henderson, *Phys. Chem. Chem. Phys.* **2004**, *6*, 4260.
[40] P. Johansson, J. Grondin, J.-C. Lassègues, *J. Phys. Chem. A* **2010**, *114*, 10700.
[41] R. Tatara, Y. Yu, P. Karayaylali, A. K. Chan, Y. Zhang, R. Jung, F. Maglia, L. Giordano, Y. Shao-Horn, *ACS Appl. Mater. Interfaces* **2019**, *11*, 34973.
[42] A. von Cresce, K. Xu, *Electrochem. Solid-State Lett.* **2011**, *14*, A154.
[43] C. Wan, M. Y. Hu, O. Borodin, J. Qian, Z. Qin, J.-G. Zhang, J. Z. Hu, *J. Power Sources* **2016**, *307*, 231.
[44] X. Bogle, R. Vazquez, S. Greenbaum, A. W. von Cresce, K. Xu, *J. Phys. Chem. Lett.* **2013**, *4*, 1664.
[45] Y. M. Cahen, P. R. Handy, E. T. Roach, A. I. Popov, *J. Phys. Chem.* **1975**, *79*, 80.
[46] C. J. Jameson, H. S. Gutowsky, *J. Chem. Phys.* **1964**, *40*, 1714.
[47] M. S. Whittingham, *Chem. Rev.* **2004**, *104*, 4271.
[48] M. S. Whittingham, *Chem. Rev.* **2014**, *114*, 11414.
[49] H. Gao, B. Gallant, *Nat. Rev. Chem.* **2020**, *4*, 566.
[50] L. Johnson, C. Li, Z. Liu, Y. Chen, S. A. Freunberger, P. C. Ashok, B. B. Praveen, K. Dholakia, J.-M. Tarascon, P. G. Bruce, *Nat. Chem.* **2014**, *6*, 1091.
[51] C. O. Laoire, S. Mukerjee, K. M. Abraham, E. J. Plichta, M. A. Hendrickson, *J. Phys. Chem. C* **2010**, *114*, 9178.
[52] W. Xu, J. Xiao, D. Wang, J. Zhang, J.-G. Zhang, *J. Electrochem. Soc.* **2010**, *157*, A219.
[53] N. B. Aetukuri, B. D. McCloskey, J. M. García, L. E. Krupp, V. Viswanathan, A. C. Luntz, *Nat. Chem.* **2015**, *7*, 50.
[54] T. P. Batcho, G. Leverick, Y. Shao-Horn, C. V. Thompson, *J. Phys. Chem. C* **2019**, *123*, 14272.
[55] Q. Xiong, C. Li, Z. Li, Y. Liang, J. Li, J. Yan, G. Huang, X. Zhang, *Adv. Mater.* **2022**, *34*, 2110416.
[56] R. Kumar, J. Liu, J.-Y. Hwang, Y.-K. Sun, *J. Mater. Chem. A* **2018**, *6*, 11582.
[57] C. Shen, J. Xie, M. Zhang, P. Andrei, M. Hendrickson, E. J. Plichta, J. P. Zheng, *Electrochim. Acta* **2017**, *248*, 90.
[58] A. Manthiram, Y. Fu, Y.-S. Su, *Acc. Chem. Res.* **2013**, *46*, 1125.
[59] S. Jeschke, P. Johansson, *Chem. - Eur. J.* **2017**, *23*, 9130.
[60] D. Zheng, X. Zhang, C. Li, M. E. McKinnon, R. G. Sadok, D. Qu, X. Yu, H.-S. Lee, X.-Q. Yang, D. Qu, *J. Electrochem. Soc.* **2015**, *162*, A203.
[61] Z. Li, Y. Zhou, Y. Wang, Y.-C. Lu, *Adv. Energy Mater.* **2019**, *9*, 1802207.
[62] G. Leverick, Y. G. Zhu, S. Lohmar, F. Bardé, S. Cotte, Y. Shao-Horn, *J. Phys. Chem. C* **2022**, *126*, 8256.
[63] T. Umezawa, S. Tatuoka, *Jpn. J. Appl. Phys.* **1972**, *11*, 906.
[64] P. M. Sipos, G. Hefter, P. M. May, *J. Chem. Eng. Data* **2000**, *45*, 613.
[65] M. Uematsu, E. U. Frank, *J. Phys. Chem. Ref. Data* **1980**, *9*, 1291.
[66] X. Yu, Z. Bi, F. Zhao, A. Manthiram, *Adv. Energy Mater.* **2016**, *6*, 1601392.
[67] X. Zhang, Q. Jin, Y. Nan, L. Hou, B. Li, X. Chen, Z. Jin, X. Zhang, J. Huang, Q. Zhang, *Angew. Chem., Int. Ed.* **2021**, *60*, 15503.
[68] M. Yanagi, K. Ueno, A. Ando, S. Li, Y. Matsumae, J. Liu, K. Dokko, M. Watanabe, *J. Electrochem. Soc.* **2020**, *167*, 070531.
[69] L. Cheng, L. A. Curtiss, K. R. Zavadil, A. A. Gewirth, Y. Shao, K. G. Gallagher, *ACS Energy Lett.* **2016**, *1*, 503.
[70] B. D. McCloskey, A. Speidel, R. Scheffler, D. C. Miller, V. Viswanathan, J. S. Hummelshøj, J. K. Nørskov, A. C. Luntz, *J. Phys. Chem. Lett.* **2012**, *3*, 997.
[71] S. Feng, M. Chen, L. Giordano, M. Huang, W. Zhang, C. V. Amanchukwu, R. Anandakathir, Y. Shao-Horn, J. A. Johnson, *J. Mater. Chem. A* **2017**, *5*, 23987.
[72] S. Feng, M. Huang, J. R. Lamb, W. Zhang, R. Tatara, Y. Zhang, Y. Guang Zhu, C. F. Perkinson, J. A. Johnson, Y. Shao-Horn, *Chem* **2019**, *5*, 2630.
[73] W. Xue, Z. Shi, M. Huang, S. Feng, C. Wang, F. Wang, J. Lopez, B. Qiao, G. Xu, W. Zhang, Y. Dong, R. Gao, Y. Shao-Horn, J. A. Johnson, J. Li, *Energy Environ. Sci.* **2020**, *13*, 212.
[74] A. Schürmann, B. Luerßen, D. Mollenhauer, J. Janek, D. Schröder, *Chem. Rev.* **2021**, *121*, 12445.
[75] L. Suo, O. Borodin, T. Gao, M. Olguin, J. Ho, X. Fan, C. Luo, C. Wang, K. Xu, *Science* **2015**, *350*, 938.
[76] K. Matsumoto, K. Inoue, K. Nakahara, R. Yuge, T. Noguchi, K. Utsugi, *J. Power Sources* **2013**, *231*, 234.
[77] S.-K. Jeong, M. Inaba, Y. Iriyama, T. Abe, Z. Ogumi, *Electrochem. Solid-State Lett.* **2003**, *6*, A13.

[78] Y. Yamada, K. Furukawa, K. Sodeyama, K. Kikuchi, M. Yaegashi, Y. Tateyama, A. Yamada, *J. Am. Chem. Soc.* **2014**, *136*, 5039.
[79] N. Mozhzhukhina, L. P. Méndez De Leo, E. J. Calvo, *J. Phys. Chem. C* **2013**, *117*, 18375.
[80] D. G. Kwabi, T. P. Batcho, C. V. Amanchukwu, N. Ortiz-Vitoriano, P. Hammond, C. V. Thompson, Y. Shao-Horn, *J. Phys. Chem. Lett.* **2014**, *5*, 2850.
[81] D. Sharon, M. Afri, M. Noked, A. Garsuch, A. A. Frimer, D. Aurbach, *J. Phys. Chem. Lett.* **2013**, *4*, 3115.
[82] T. M. Østergaard, L. Giordano, I. E. Castelli, F. Maglia, B. K. Antonopoulos, Y. Shao-Horn, J. Rossmeisl, *J. Phys. Chem. C* **2018**, *122*, 10442.
[83] V. Pande, V. Viswanathan, *J. Phys. Chem. Lett.* **2019**, *10*, 7031.
[84] O. Borodin, J. Self, K. A. Persson, C. Wang, K. Xu, *Joule* **2020**, *4*, 69.
[85] K. Dokko, N. Tachikawa, K. Yamauchi, M. Tsuchiya, A. Yamazaki, E. Takashima, J.-W. Park, K. Ueno, S. Seki, N. Serizawa, M. Watanabe, *J. Electrochem. Soc.* **2013**, *160*, A1304.
[86] S. Chen, J. Zheng, D. Mei, K. S. Han, M. H. Engelhard, W. Zhao, W. Xu, J. Liu, J. Zhang, *Adv. Mater.* **2018**, *30*, 1706102.
[87] D. G. Kwabi, T. P. Batcho, S. Feng, L. Giordano, C. V. Thompson, Y. Shao-Horn, *Phys. Chem. Chem. Phys.* **2016**, *18*, 24944.
[88] Y. G. Zhu, Q. Liu, Y. Rong, H. Chen, J. Yang, C. Jia, L.-J. Yu, A. Karton, Y. Ren, X. Xu, S. Adams, Q. Wang, *Nat. Commun.* **2017**, *8*, 14308.
[89] T. Liu, G. Kim, E. Jónsson, E. Castillo-Martinez, I. Temprano, Y. Shao, J. Carretero-González, R. N. Kerber, C. P. Grey, *ACS Catal.* **2018**, *9*, 66.
[90] M. Tułodziecki, G. M. Leverick, C. V. Amanchukwu, Y. Katayama, D. G. Kwabi, F. Bardé, P. T. Hammond, Y. Shao-Horn, *Energy Environ. Sci.* **2017**, *10*, 1828.
[91] Y. Zhang, *Revealing Interfacial Reactions and Charge Transfer Kinetics in Electrochemical Energy Storage and Conversion, Ph.D. Thesis*, MIT, XX **2022**.
[92] N. Dubouis, A. Serva, R. Berthin, G. Jeanmairet, B. Porcheron, E. Salager, M. Salanne, A. Grimaud, *Nat. Catal.* **2020**, *3*, 656.
[93] P. C. F. Pau, J. O. Berg, W. G. McMillan, *J. Phys. Chem.* **1990**, *94*, 2671.
[94] J. M. Tarascon, D. Guyomard, *Solid State Ionics* **1994**, *69*, 293.
[95] R. Fong, U. von Sacken, J. R. Dahn, *J. Electrochem. Soc.* **1990**, *137*, 2009.
[96] T. Zhang, E. Paillard, *Front Chem Sci Eng* **2018**, *12*, 577.
[97] K. Xu, *J. Electrochem. Soc.* **2007**, *154*, A162.
[98] J. Ming, Z. Cao, Y. Wu, W. Wahyudi, W. Wang, X. Guo, L. Cavallo, J.-Y. Hwang, A. Shamim, L.-J. Li, Y.-K. Sun, H. N. Alshareef, *ACS Energy Lett.* **2019**, *4*, 2613.
[99] Y. Yao, X. Chen, C. Yan, X. Zhang, W. Cai, J. Huang, Q. Zhang, *Angew. Chem., Int. Ed.* **2021**, *60*, 4090.
[100] C. Su, M. He, J. Shi, R. Amine, J. Zhang, K. Amine, *Angew. Chem., Int. Ed.* **2020**, *59*, 18229.
[101] X.-Q. Zhang, X. Chen, X.-B. Cheng, B.-Q. Li, X. Shen, C. Yan, J.-Q. Huang, Q. Zhang, *Angew. Chem., Int. Ed.* **2018**, *57*, 5301.
[102] Z. Wang, F. Qi, L. Yin, Y. Shi, C. Sun, B. An, H. Cheng, F. Li, *Adv. Energy Mater.* **2020**, *10*, 1903843.
[103] S. Sun, G. Kim, D. Lee, E. Park, S. Myeong, B. Son, K. Lee, M. Jang, U. Paik, T. Song, *Chem. Commun.* **2022**, *58*, 9834.
[104] J. He, H. Wang, Q. Zhou, S. Qi, M. Wu, F. Li, W. Hu, J. Ma, *Small Methods* **2021**, *5*, 2100441.
[105] C. Jiang, Q. Jia, M. Tang, K. Fan, Y. Chen, M. Sun, S. Xu, Y. Wu, C. Zhang, J. Ma, C. Wang, W. Hu, *Angew. Chem., Int. Ed.* **2021**, *60*, 10871.
[106] K. S. Jiang, G. M. Hobold, R. Guo, K.-H. Kim, A. M. Melemed, D. Wang, L. Zuin, B. M. Gallant, *ACS Energy Lett.* **2022**, *7*, 3378.
[107] F. Liu, G. Sun, H. B. Wu, G. Chen, D. Xu, R. Mo, L. Shen, X. Li, S. Ma, R. Tao, X. Li, X. Tan, B. Xu, G. Wang, B. S. Dunn, P. Sautet, Y. Lu, *Nat. Commun.* **2020**, *11*, 5215.
[108] Y. Tsao, M. Lee, E. C. Miller, G. Gao, J. Park, S. Chen, T. Katsumata, H. Tran, L.-W. Wang, M. F. Toney, Y. Cui, Z. Bao, *Joule* **2019**, *3*, 872.
[109] Y. Peng, M. Zhao, Z. Chen, Q. Cheng, Y. Liu, C. Zhao, X. Ma, B. Li, C. Chen, J. Huang, Q. Zhang, *Batteries Supercaps.* **2022**, *5*, 202100359.
[110] X. Gao, Y. Chen, L. R. Johnson, Z. P. Jovanov, P. G. Bruce, *Nat. Energy* **2017**, *2*, 17118.
[111] Z. Liang, Y. Zhou, Y.-C. Lu, *Energy Environ. Sci.* **2018**, *11*, 3500.
[112] J. Li, S. Ding, S. Zhang, W. Yan, Z.-F. Ma, X. Yuan, L. Mai, J. Zhang, *Energy Storage Mater.* **2021**, *43*, 97.
[113] A. Tkacheva, B. Sun, J. Zhang, G. Wang, A. M. McDonagh, *J. Phys. Chem. C* **2021**, *125*, 2824.
[114] M. Balaish, X. Gao, P. G. Bruce, Y. Ein-Eli, *Adv. Mater. Technol.* **2019**, *4*, 1800645.
[115] V. Giordani, D. Tozier, J. Uddin, H. Tan, B. Gallant, B. McCloskey, J. Greer, G. Chase, D. Addison, *Nat. Chem.* **2019**, *11*, 1133.
[116] Y. G. Zhu, G. Leverick, A. Accogli, K. Gordiz, Y. Zhang, Y. Shao-Horn, *Energy Environ. Sci.* **2022**, *15*, 4636.
[117] Y. G. Zhu, G. Leverick, L. Giordano, S. Feng, Y. Zhang, Y. Yu, R. Tatara, J. R. Lunger, Y. Shao-Horn, *Joule* **2022**, *6*, 1887.
[118] V. Giordani, D. Tozier, H. Tan, C. M. Burke, B. M. Gallant, J. Uddin, J. R. Greer, B. D. McCloskey, G. V. Chase, D. Addison, *J. Am. Chem. Soc.* **2016**, *138*, 2656.
[119] C. Xia, C. Y. Kwok, L. F. Nazar, *Science* **2018**, *361*, 777.
[120] X. Gao, Y. Chen, L. Johnson, P. G. Bruce, *Nat. Mater.* **2016**, *15*, 882.
[121] Y. Chen, S. A. Freunberger, Z. Peng, O. Fontaine, P. G. Bruce, *Nat. Chem.* **2013**, *5*, 489.
[122] K. P. C. Yao, M. Risch, S. Y. Sayed, Y.-L. Lee, J. R. Harding, A. Grimaud, N. Pour, Z. Xu, J. Zhou, A. Mansour, F. Bardé, Y. Shao-Horn, *Energy Environ. Sci.* **2015**, *8*, 2417.
[123] Z. Liang, Y.-C. Lu, *J. Am. Chem. Soc.* **2016**, *138*, 7574.
[124] H.-M. Kwon, M. L. Thomas, R. Tatara, A. Nakanishi, K. Dokko, M. Watanabe, *Chem. Lett.* **2017**, *46*, 573.
[125] R. A. Wong, C. Yang, A. Dutta, M. O. , M. Hong, M. L. Thomas, K. Yamanaka, T. Ohta, K. Waki, H. R. Byon, *ACS Energy Lett.* **2018**, *3*, 592.
[126] M. D. Radin, D. J. Siegel, *Energy Environ. Sci.* **2013**, *6*, 2370.
[127] B. J. Bergner, A. Schürmann, K. Peppler, A. Garsuch, J. Janek, *J. Am. Chem. Soc.* **2014**, *136*, 15054.
[128] D. Kundu, R. Black, B. Adams, L. F. Nazar, *ACS Cent. Sci.* **2015**, *1*, 510.
[129] W. R. Torres, S. E. Herrera, A. Y. Tesio, M. del Pozo, E. J. Calvo, *Electrochim. Acta* **2015**, *182*, 1118.
[130] H.-D. Lim, H. Song, J. Kim, H. Gwon, Y. Bae, K.-Y. Park, J. Hong, H. Kim, T. Kim, Y. H. Kim, X. Lepró, R. Ovalle-Robles, R. H. Baughman, K. Kang, *Angew. Chem., Int. Ed.* **2014**, *53*, 3926.
[131] W.-J. Kwak, D. Hirshberg, D. Sharon, M. Afri, A. A. Frimer, H.-G. Jung, D. Aurbach, Y.-K. Sun, *Energy Environ. Sci.* **2016**, *9*, 2334.
[132] G. Leverick, M. Tułodziecki, R. Tatara, F. Barde´, Y. Shao-Horn, *Joule* **2019**, *3*, 1106.
[133] T. Liu, M. Leskes, W. Yu, A. J. Moore, L. Zhou, P. M. Bayley, G. Kim, C. P. Grey, *Science* **2015**, *350*, 530.
[134] C. L. Bentley, A. M. Bond, A. F. Hollenkamp, P. J. Mahon, J. Zhang, *J. Phys. Chem. C* **2015**, *119*, 22392.
[135] A. Nakanishi, M. L. Thomas, H.-M. Kwon, Y. Kobayashi, R. Tatara, K. Ueno, K. Dokko, M. Watanabe, *J. Phys. Chem. C* **2018**, *122*, 1522.
[136] X.-Q. Zhu, C.-H. Wang, *J. Org. Chem.* **2010**, *75*, 5037.
[137] G. Leverick, S. Feng, P. Acosta, S. Acquaviva, F. Bardé, S. Cotte, Y. Shao-Horn, *ACS Appl. Mater. Interfaces* **2022**, *14*, 6689.
[138] C. L. Bentley, A. M. Bond, A. F. Hollenkamp, P. J. Mahon, J. Zhang, *Anal. Chem.* **2013**, *85*, 11319.
[139] S. Zhang, Y. Yang, L. Cheng, J. Sun, X. Wang, P. Nan, C. Xie, H. Yu, Y. Xia, B. Ge, J. Lin, L. Zhang, C. Guan, G. Xiao, C. Peng, G. Z. Chen, J.-Q. Wang, *Energy Storage Mater.* **2021**, *35*, 142.

[140] D. Koo, S. J. Kang, *ACS Appl. Mater. Interfaces* **2021**, *13*, 47740.
[141] H. Zarrin, S. Farhad, F. Hamdullahpur, V. Chabot, A. Yu, M. Fowler, Z. Chen, *Electrochim. Acta* **2014**, *125*, 117.
[142] Y. Kato, S. Hori, T. Saito, K. Suzuki, M. Hirayama, A. Mitsui, M. Yonemura, H. Iba, R. Kanno, *Nat. Energy* **2016**, *1*, 16030.
[143] J. Zhu, X. Li, C. Wu, J. Gao, H. Xu, Y. Li, X. Guo, H. Li, W. Zhou, *Angew. Chem., Int. Ed.* **2021**, *60*, 3781.
[144] L. Zhou, T.-T. Zuo, C. Y. Kwok, S. Y. Kim, A. Assoud, Q. Zhang, J. Janek, L. F. Nazar, *Nat. Energy* **2022**, *7*, 83.
[145] S. Lee, C.-H. Chen, A. H. Flood, *Nat. Chem.* **2013**, *5*, 704.
[146] A. C. Kumbharkhane, S. N. Helambe, M. P. Lokhande, S. Doraiswamy, S. C. Mehrotra, *Pramana – J. Phys.* **1996**, *46*, 91.
[147] B. Qiao, G. M. Leverick, W. Zhao, A. H. Flood, J. A. Johnson, Y. Shao-Horn, *J. Am. Chem. Soc.* **2018**, *140*, 10932.
[148] B. Qiao, S. Mohapatra, J. Lopez, G. M. Leverick, R. Tatara, Y. Shibuya, Y. Jiang, A. France-Lanord, J. C. Grossman, R. Gómez-Bombarelli, J. A. Johnson, Y. Shao-Horn, *ACS Cent. Sci.* **2020**, *6*, 1115.
[149] J. -H. Chen, S. A. Adelman, *J. Chem. Phys.* **1980**, *72*, 2819.
[150] P. Colonomos, P. G. Wolynes, *J. Chem. Phys.* **1979**, *71*, 2644.
[151] K. Dokko, D. Watanabe, Y. Ugata, M. L. Thomas, S. Tsuzuki, W. Shinoda, K. Hashimoto, K. Ueno, Y. Umebayashi, M. Watanabe, *J. Phys. Chem. B* **2018**, *122*, 10736.
[152] Y. Ugata, G. Hasegawa, N. Kuwata, K. Ueno, M. Watanabe, K. Dokko, *J. Phys. Chem. C* **2022**, *126*, 19084.
[153] O. Borodin, G. D. Smith, *J. Solution Chem.* **2007**, *36*, 803.
[154] K.-D. Kreuer, S. J. Paddison, E. Spohr, M. Schuster, *Chem. Rev.* **2004**, *104*, 4637.
[155] N. Agmon, *Chem. Phys. Lett.* **1995**, *244*, 456.
[156] K. Tasaki, A. Goldberg, J.-J. Lian, M. Walker, A. Timmons, S. J. Harris, *J. Electrochem. Soc.* **2009**, *156*, A1019.
[157] S. Jurng, Z. L. Brown, J. Kim, B. L. Lucht, *Energy Environ. Sci.* **2018**, *11*, 2600.
[158] R. Guo, K.-H. Kim, B. M. Gallant, *J. Electrochem. Soc.* **2022**, *169*, 100523.
[159] D. Fraggedakis, M. McEldrew, R. B. Smith, Y. Krishnan, Y. Zhang, P. Bai, W. C. Chueh, Y. Shao-Horn, M. Z. Bazant, *Electrochim. Acta* **2021**, *367*, 137432.
[160] G. M. Hobold, K.-H. Kim, B. M. Gallant, *Benefic. Chem.* **2022**, https://doi.org/10.26434/chemrxiv-2022-j04d3.
[161] Y. Liu, X. Xu, M. Sadd, O. O. Kapitanova, V. A. Krivchenko, J. Ban, J. Wang, X. Jiao, Z. Song, J. Song, S. Xiong, A. Matic, *Adv. Sci.* **2021**, *8*, 2003301.
[162] D. T. Boyle, X. Kong, A. Pei, P. E. Rudnicki, F. Shi, W. Huang, Z. Bao, J. Qin, Y. Cui, *ACS Energy Lett.* **2020**, *5*, 701.
[163] Y. Yamada, Y. Iriyama, T. Abe, Z. Ogumi, *Langmuir* **2009**, *25*, 12766.
[164] K. Xu, A. von Cresce, U. Lee, *Langmuir* **2010**, *26*, 11538.
[165] Y. Li, Y. Qi, *Energy Environ. Sci.* **2019**, *12*, 1286.
[166] Y. Mizuno, M. Okubo, E. Hosono, T. Kudo, H. Zhou, K. Oh-ishi, *J. Phys. Chem. C* **2013**, *117*, 10877.
[167] V. A. Nikitina, S. Y. Vassiliev, K. J. Stevenson, *Adv. Energy Mater.* **2020**, *10*, 1903933.
[168] Y. Marcus, *Pure Appl. Chem.* **1983**, *55*, 977.
[169] P. M. Chekushkin, I. S. Merenkov, V. S. Smirnov, S. A. Kislenko, V. A. Nikitina, *Electrochim. Acta* **2021**, *372*, 137843.
[170] C. D. Parke, L. Teo, D. T. Schwartz, V. R. Subramanian, *Sustainable Energy Fuels* **2021**, *5*, 5946.
[171] A. Wang, S. Kadam, H. Li, S. Shi, Y. Qi, *npj Comput. Mater.* **2018**, *4*, 15.

Graham Leverick is currently a postdoctoral associate at MIT. He received his B.Sc. and M.Sc. in Mechanical Engineering at the University of Manitoba and his Ph.D. from MIT under the supervision of Prof. Shao-Horn. His research focuses on leveraging electrolyte design to enable next-generation batteries and electrochemical devices, as well as carbon capture and utilization.

Shao-Horn is a member of the National Academy of Engineering. She is a fellow of the American Association for the Advancement of Science, the Electrochemical Society, the National Academy of Inventors and the International Society of Electrochemistry. She has advised 100+ students and postdocs at MIT, who are now pursuing successful careers in industry including Telsa, Amazon and Apple, national research laboratories, and in academia (≈35) including faculty positions at MIT and academic positions in Europe and Asia.